


RESEARCH

Open Access



# An artificial neural network visible mathematical model for predicting slug liquid holdup in low to high viscosity multiphase flow for horizontal to vertical pipes

Chibuzo Cosmas Nwanwe<sup>1,2,3\*</sup> , Ugochukwu Ilozurike Duru<sup>3</sup>, Charley Lyke C. Anyadiiegwu<sup>3</sup>, Azunna I. B. Ekejuba<sup>3</sup>, Stanley I. Onwukwe<sup>3</sup>, Angela N. Nwachukwu<sup>3</sup> and Boniface U. Okonkwo<sup>4</sup>

\*Correspondence:  
nwanwe.chibuzo@fpno.edu.ng;  
cnwanwe@ttu.edu

<sup>1</sup> Department of Mineral and Petroleum Resources Engineering Technology, Federal Polytechnic Nekede, Owerri P.M.B. 1036, Imo, Nigeria

<sup>2</sup> Bob L. Herd Department of Petroleum Engineering, Texas Tech University, Lubbock, TX 79049, USA

<sup>3</sup> Department of Petroleum Engineering, Federal University of Technology, Owerri P.M.B. 1526, Imo, Nigeria

<sup>4</sup> Department of Mechanical Engineering, Federal University of Technology, Owerri P.M.B. 1526, Imo, Nigeria

## Abstract

Slug liquid holdup (SLH) is a critical requirement for accurate pressure drop prediction during multiphase pipe flows and by extension optimal gas lift design and production optimization in wellbores. Existing empirical correlations provide inaccurate predictions because they were developed with regression analysis and data measured for limited ranges of flow conditions. Existing SLH machine learning models provide accurate predictions but are published without any equations making their use by other researchers difficult. The only existing ML model published with actual equations cannot be considered optimum because it was selected by considering artificial neural network (ANN) structures with only one hidden layer. In this study, an ANN-based model for SLH prediction with actual equations is presented. A total of 2699 data points randomly divided into 70%, 15%, and 15% for training, validation, and testing was used in constructing 71 different network structures with 1, 2, and 3 hidden layers respectively. Sensitivity analysis revealed that the optimum network structure has 3 hidden layers with 20, 5, and 15 neurons in the first, second, and third hidden layers, respectively. The optimum network structure was translated into actual equations with the aid of the weights, biases, and activation functions. Trend analysis revealed that this study's model reproduced the expected effects of inputs on SLH. Test against measured data revealed that this study's model is in agreement with measured data with coefficient of determinations of 0.9791, 0.9727, 0.9756, and 0.9776 for training, testing, validation, and entire datasets, respectively. Comparative study revealed that this study's model outperformed existing models with a relative performance factor of 0.002. The present model is presented with visible mathematical equations making its implementation by any user easy and without the need for any ML framework. Unlike existing ANN-based models developed with one hidden layered ANN structures, the present model was developed by considering ANN structures with one, two, and three hidden layers, respectively.

**Keywords:** Artificial neural network, Slug liquid holdup, Visible mathematical model, Black-box model, Linear activation function, Hyperbolic tangent activation function, Levenberg–Marquardt optimization algorithm

## Introduction

Multiphase flow in pipes is the simultaneous flow of more than one phase in pipes [1] and is commonly encountered in the petroleum production, drilling, processing, and transportation systems [2, 3]. Multiphase flow modeling is more complex than single-phase flow modeling due to the difficulty in identifying flow patterns present during multiphase flow [4].

Flow patterns that have been reported in the literature for vertical-upward flow [5] and inclined-upward flow [6] include dispersed bubble, slug, churn, and annular flow patterns. Some investigators combined the slug and churn flow into a flow pattern referred to as an intermittent flow pattern [7]. Flow patterns reported for horizontal flow include intermittent, stratified-smooth, stratified-wave, dispersed bubble, and annular flow patterns [8]. Annular, slug, and dispersed bubble flow patterns have been observed for vertical downward flow [9], while stratified wave flow pattern has been observed as the dominant flow pattern for inclined downward flow [10].

Slug flow is one of the dominant flow patterns encountered during the multiphase flow of oil and gas in pipelines and wellbores [11] and occurs over a wide range of flow conditions. Slug flow is characterized by a series of slug units with each unit consisting of a Taylor bubble, thin liquid film, and liquid slug [12]. Slug flow develops when gas rate in the bubble flow regime is increased to a point where the bubbles become closely packed and start coalescing into larger bullet shaped bubbles called Taylor bubbles [5]. The Taylor bubbles eventually occupy the entire pipe cross section as the coalescence continues [13]. The formed Taylor bubbles are separated from the pipe wall by a thin film of liquid flowing downward relative to the Taylor bubbles. The liquid slug, carrying dispersed bubbles shed from the tail of the leading Taylor bubble [13], bridges the pipe and separates two consecutive Taylor bubbles [12]. The Taylor bubbles and small bubbles in the liquid slug in inclined pipes tend to accumulate near the upper part of the pipe section due to buoyancy resulting in a nonuniform film thickness profile across the pipe section [14].

Slug liquid holdup (SLH) is one of the critical slug flow closure correlations required for accurate prediction of pressure drop during slug flow and by extension optimal tubing design [15] and production optimization in wellbores. Other slug flow closure relationships include translational velocity and slug length [11, 16]. Comparative performance analysis of models for predicting pressure drop in vertical wells conducted by Nwanwe and Duru [17] revealed that empirical correlations outperformed mechanistic models. Further investigation revealed that pressure drop is severely under-predicted whenever slug flow pattern is predicted by these mechanistic models. It follows therefore that this severe underprediction of pressure drop is due to severe underprediction of the closure relationships of the slug flow model of these mechanistic models. SLH is the slug flow closure correlation of focus for the current study.

The models developed over the years for the prediction of SLH can be categorized as empirical correlations [18–24], semi-mechanistic models [25, 26], mechanistic models [27, 28], and most recently machine learning models [29, 30]. All these SLH models with the exception of the machine learning models were developed with the aid of regression analysis-based laboratory dataset measured for narrow range flow conditions. These models are applicable for either low viscosity slug flow conditions [18, 23, 31–33], high

viscosity horizontal slug flow conditions [20, 21, 24], high viscosity vertical slug flow conditions [34], high viscosity horizontal to vertical slug flow conditions [19], or low viscosity to high viscosity horizontal to vertical slug flow conditions [30].

In this study, a literature review conducted identified some issues with existing models for predicting SLH during multiphase flow in pipes. First, existing SLH empirical correlations, semi-mechanistic models, and mechanistic models have failed to produce accurate SLH predictions. This is because these correlations and models were developed using regression analysis which is incapable of adequately capturing the nonlinearity between the independent variables and dependent variable. In addition, none of these correlations and models was developed with data measured for low to high viscosity horizontal to vertical upward flow conditions. Hence, these correlations and models failed when applied to flow conditions different from those employed in their formulation. Second, to the authors' knowledge, the Abdul-Majeed et al. model [30] is the only SLH model developed with artificial neural network (ANN) and with data measured for low viscosity to high viscosity horizontal to vertical slug flow conditions. However, in selecting the optimum network structure, the authors [30] only considered a network structure with a single hidden layer (HL). They used a program that performed checks on the number of neurons and their weights in the single HL and then selected the network structure with the lowest mean square error as optimum. The structure selected by these authors as optimum contains 11 neurons in the single HL. This selected network structure cannot be considered as optimum because the authors only considered one HL in their selection. ANN and adaptive neuro-fuzzy inference system (ANFIS) has been used to solve complex problems in the petroleum industry, but only few of these studies have developed and presented as a visible mathematical model [35–38].

In the present study, a slug liquid holdup artificial neural network visible mathematical model (SLH-ANN-VMM) applicable for low to high viscosity horizontal to vertical upward pipe flow conditions is proposed. A dataset consisting of 2699 data points collected from open source [39] was used for the model development. A total of 70% of the dataset was used for training and 15% for testing and validation respectively. The training dataset was transformed into four dimensionless numbers [40] and an inclination angle. This was followed by the application of the dimensionless transformation to the testing and validation datasets. The entire dataset was used in the construction of 71 different network structures with each structure having either 1, 2, or 3 HLs with varying numbers of neurons in each HL. Sensitivity analysis was performed for the 71 network structures, and the optimum network structure selected was based on three statistical performance indicators, namely correlation coefficient, mean square error, and relative performance factor. A structure is considered optimum if it achieved best performance with respect to two or all three statistical performance indicators. The network structure selected as optimum in this study contains 20 neurons in the first HL, 5 in the second HL, and 15 in the third HL. The trained SLH-ANN black-box model (BBM) was translated into a SLH-ANN-VMM with the aid of the extracted tuned biases and weights and the activation functions. The SLH-ANN-VMM was also written in a MATLAB code. Three evaluation tests were performed. First, trend analysis revealed that the proposed SLH-ANN-VMM produced the expected effect of various independent variables on the SLH. Second, the test against measured dataset revealed that the SLH predicted by the

proposed SLH-ANN-VMM is in close agreement with the measured SLH. Third, the comparative study revealed that the proposed SLH-ANN-VMM outperformed existing SLH models.

## Methods

### Data collection and description

Openly sourced datasets consisting of 2669 data points collected from 23 different studies and published as an open source Mendeley Data [39] were used in developing the proposed slug liquid holdup artificial neural network visible mathematical model (SLH-ANN-VMM). The dataset is made of seven input variables and one output variable. The input variables include superficial gas velocity ( $V_{SG}$ ), superficial liquid velocity ( $V_{SL}$ ), liquid viscosity ( $\mu_L$ ), internal diameter of pipe ( $d$ ), liquid density ( $\rho_L$ ), inclination angle ( $\theta$ ), and surface tension ( $\sigma_L$ ). The slug liquid holdup ( $H_{LS}$ ) is the output variable. Description of the entire dataset employed in the present is as shown in Table 1.

### Data preprocessing

Abdul-Majeed et al. [30] demonstrated based on measured data that SLH,  $H_{LS}$ , is strongly affected by superficial gas velocity,  $V_{SG}$ , superficial liquid velocity,  $V_{SL}$ , liquid viscosity,  $\mu_L$ , pipe internal diameter,  $d$ , pipe inclination angle,  $\theta$ , and surface tension,  $\sigma_L$ , respectively. The authors went further to develop a single hidden layer ANN-VMM for  $H_{LS}$  prediction as function of  $V_{SL}$ ,  $V_{SG}$ ,  $\mu_L$ ,  $d$ ,  $\theta$ , and  $\sigma_L$ , while liquid density,  $\rho_L$ , was neglected. Other authors used regression analysis to developed  $H_{LS}$  models as function of Wallis [41] dimensionless Froude number,  $N_{Fr}$ , and viscosity number,  $N_\mu$  [20, 21, 24] and  $N_{Fr}$ , and inverse of the viscosity number,  $N_f$  [34],  $N_{Fr}$ ,  $N_\mu$ , and  $\theta$  [19]. Recent studies [42, 43] revealed that the use of dimensionless numbers leads to poorer accuracy compared to using the entire set of parameters.

The use of  $\theta$  and any two of  $N_{Fr}$ ,  $N_\mu$  and  $N_f$ , accounts for all input variables used by Abdul-Majeed et al. [30] with exception of  $\sigma_L$ . We propose using  $\theta$  and the four dimensionless numbers as originally proposed by Ros [40] to account for the effect of all input variables including  $\sigma_L$  and  $\rho_L$  in training the ANN. The Ros [40] gas velocity number, liquid velocity number, pipe diameter number, and liquid viscosity number employed in this study are as given in Eqs. (1), (2), (3), and (4) in metric units respectively. The statistical analysis of the preprocessed dataset is as shown in Table 2.

**Table 1** Description of the entire dataset (2699 data points) employed in the present study

S/N	Variables	Units	Min	Max	Average	Std
1	Superficial gas velocity, $V_{SG}$	$m/s$	0.030	15.308	1.848	2.181
2	Superficial liquid velocity, $V_{SL}$	$m/s$	0.011	3.048	0.500	0.489
3	Liquid viscosity, $\mu_L$	$mPas$	1.000	5300.000	323.931	739.984
4	Pipe internal diameter, $d$	$m$	0.023	0.100	0.052	0.018
5	Liquid density, $\rho_L$	$kg/m^3$	795.748	1300.000	883.136	83.521
6	Pipe inclination angle, $\theta$	$^\circ$	0.000	90.000	14.660	29.284
7	Surface tension, $\sigma_L$	$mN/m$	27.500	72.000	31.632	7.789
8	Slug liquid holdup, $H_{LS}$	-	0.164	1.000	0.820	0.189

**Table 2** Description of the preprocessed dataset (2699 data points) employed in the present research

S/N	Variables	Units	Min	Max	Average	Std
1	Gas velocity number, $N_{GV}$	-	0.2221	112.5366	13.5169	15.9312
2	Liquid velocity number, $N_{LV}$	-	0.0821	22.4073	3.6624	3.5720
3	Pipe diameter number, $N_d$	-	12.2862	54.3110	27.5472	9.3368
4	Liquid viscosity number, $N_L$	-	0.2240	2086.4874	131.3393	292.4623
5	Inclination angle, $\theta$	°	0.0000	90.0000	14.6602	29.2836
6	Slug liquid holdup, $H_{LS}$	-	0.1640	1.0000	0.8197	0.1887

**Table 3** Parameter ranges for the training, validation, and testing datasets employed in the present study

S/N	Parameters	Units	Training dataset (1889 data points)		Testing dataset (405 data points)		Validation dataset (405 data points)	
			Min	Max	Min	Max	Min	Max
1	Gas velocity number, $N_{GV}$	-	0.2221	112.5366	0.7218	95.8498	0.2221	76.8864
2	Liquid velocity number, $N_{LV}$	-	0.0821	22.4073	0.2205	22.2692	0.1137	17.1699
3	Pipe diameter number, $N_d$	-	12.2862	54.3110	13.6814	28.4472	12.2862	27.6279
4	Liquid viscosity number, $N_L$	-	0.2240	2086.4874	0.5333	235.0331	0.6138	1377.8690
5	Inclination angle, $\theta$	°	0.0000	90.0000	0.0000	90.0000	0.0000	90.0000
6	Slug liquid holdup, $H_{LS}$	-	0.1640	1.0000	0.1700	0.9999	0.2070	1.0000

$$N_{GV} = 1.7964 V_{SG} \left( \frac{\rho_L}{\sigma_L} \right)^{0.25} \tag{1}$$

$$N_{LV} = 1.7964 V_{SL} \left( \frac{\rho_L}{\sigma_L} \right)^{0.25} \tag{2}$$

$$N_d = 31.664d \left( \frac{\rho_L}{\sigma_L} \right)^{0.5} \tag{3}$$

$$N_L = 0.55646 \mu_L \left( \frac{1}{\rho_L \sigma_L^3} \right)^{0.25} \tag{4}$$

**Slug liquid holdup ANN black-box model development**

A total of 2699 openly sourced laboratory-measured data points were employed in the development with the SLH-ANN-BBM. First, the dataset was preprocessed by transforming the input variables in four dimensionless numbers. Second, the preprocessed dataset was divided into three different sets: 70%, 15%, and 15% for training, testing, and validation respectively. As shown in Table 3, the division of the preprocessed dataset

ensured that all the parameter ranges in the testing and validation datasets were covered in the training dataset.

The optimum network structure was selected by first constructing 71 network structures as shown in column 2 of Table 4 with each structure having either 1, 2, or 3 hidden layers (HLs) with varying numbers of neurons in each HL. In addition, each HL consists of varying numbers of neurons ranging from 5 to 20 in steps of 5. As shown in Table 4, column 2, the figures after the letter “n” represent the neurons in the HLs. For example, the network structure n-10–20-5 is a 3 HL network with 10 neurons in the first HL, 20 in the second HL, and 5 in the third HL.

The preprocessed data points were employed in the training, testing, and validation of each of the 71 constructed network structures. We used the training dataset (1889 data points) to train each network structure until 3 basic conditions were satisfied. First, the training dataset mean square error (MSE) must be less than that of validation and testing. Second, testing and validation datasets MSE must have identical characteristics. Last, correlation coefficients must increase in the order of testing, validation, entire, and training datasets [44].

At the end of the satisfactory training of each network structure, the trained network is used in the prediction of SLH for the entire dataset (2699 data points). The predicted SLHs are then used to calculate the performance of each of the 71 satisfactorily trained network structures using 3 different statistical performance tools. The statistical performance tools include correlation coefficient,  $R$ , root-mean-square error,  $E_{rms}$ , and relative performance factor,  $F_{rp}$ .  $F_{rp}$ , as defined in Eq. (5), includes the effect of six statistical errors ( $E_1, E_2, E_3, E_4, E_5$ , and  $E_6$ ) with a minimum of zero and a maximum of six representing the best and worst performance respectively.  $E_{rms}$ , as defined in Eq. (6), with the lowest and highest values indicates best and worst performance, respectively.  $R$ , as defined in Eq. (7), with the lowest and highest values represents the worst and best performance respectively.

Table 4 presents the results of the comparative performance analysis of the 71 different network structures. As shown in Table 4, the statistical error parameters  $E_1$  through  $E_6$  are presented in columns 3 through 8. The statistical performance tools  $E_{rms}$  is presented in column 9,  $R$  in column 10, and  $F_{rp}$  in column 11. The blue cells with metrics written in white represent best performance for each considered statistical error parameter or statistical performance tool. In this study, we considered a network structure to be optimum if it achieved best performance in respect to at least two of the three statistical performance tools.

As shown in Table 4, the n-20–5-15 network structure was selected as optimum because it achieved the highest value of  $R$  (0.978), lowest value of  $E_{rms}$  (0.048), and second minimum value of  $F_{rp}$  (0.330). Levenberg–Marquardt optimization algorithm was used in training the network, the hyperbolic tangent activation function for activating the HLs, and linear activation function for activating the output layer. As shown in Fig. 1, the optimum network consists of an input layer with 5 input variables; 3 HLs with 20, 5, and 15 neurons in the first, second, and third HLs respectively; and an output layer with 1 output variable.

$$F_{rp} = \frac{|E_1| - |E_{1min}|}{|E_{1max}| - |E_{1min}|} + \frac{E_2 - E_{2min}}{E_{2max} - E_{2min}} + \frac{E_3 - E_{3min}}{E_{3max} - E_{3min}} + \frac{|E_4| - |E_{4min}|}{|E_{4max}| - |E_{4min}|} + \frac{E_5 - E_{5min}}{E_{5max} - E_{5min}} + \frac{E_6 - E_{6min}}{E_{6max} - E_6} \quad (5)$$

**Table 4** Comparative performance analysis of the 71 network structures based on the entire dataset (2699 data points)

S/N	Network Structure	$E_1$ (%)	$E_2$ (%)	$E_3$ (%)	$E_4$ (-)	$E_5$ (-)	$E_6$ (-)	$E_{rms}$ (-)	$R$ (-)	$F_{TP}$ (-)
1	n-5	-1.114	6.866	57.330	0.0002	0.046	2.366	0.117	0.880	5.183
2	n-10	-0.845	5.808	43.467	-0.0001	0.040	2.068	0.094	0.918	3.866
3	n-15	-0.652	4.701	33.530	-0.0008	0.032	1.682	0.080	0.939	3.329
4	n-20	-0.513	4.015	26.401	-0.0009	0.028	1.438	0.067	0.956	2.605
5	n-5-5	-0.710	5.470	36.545	-0.0002	0.037	1.929	0.094	0.917	3.437
6	n-10-5	-0.375	3.827	19.329	-0.0001	0.026	1.363	0.063	0.961	1.548
7	n-15-5	-0.234	3.214	12.101	0.0000	0.022	1.143	0.055	0.970	0.774
8	n-20-5	-0.338	3.097	17.432	-0.0006	0.021	1.089	0.056	0.972	1.334
9	n-5-10	-0.223	4.307	11.568	0.0010	0.030	1.531	0.071	0.950	2.350
10	n-5-15	-0.400	4.112	20.605	0.0005	0.028	1.456	0.070	0.955	2.140
11	n-5-20	-0.269	3.762	13.901	0.0003	0.025	1.319	0.063	0.962	1.463
12	n-10-10	-0.285	3.480	14.699	0.0000	0.024	1.234	0.059	0.966	1.088
13	n-15-10	-0.202	3.011	10.477	0.0001	0.020	1.049	0.060	0.972	0.614
14	n-20-10	-0.240	3.655	12.383	0.0005	0.026	1.329	0.060	0.960	1.525
15	n-10-15	-0.347	3.287	17.879	-0.0003	0.023	1.176	0.057	0.968	1.313
16	n-10-20	-0.292	3.163	15.079	-0.0002	0.022	1.125	0.055	0.971	0.958
17	n-15-15	0.056	3.188	3.418	0.0009	0.021	1.083	0.088	0.966	1.104
18	n-15-20	-0.216	3.248	11.167	-0.0002	0.022	1.169	0.054	0.969	0.938
19	n-20-15	-0.266	2.939	13.735	-0.0002	0.020	1.048	0.052	0.974	0.794
20	n-20-20	-0.262	2.782	13.531	-0.0004	0.019	0.986	0.051	0.975	0.787
21	n-5-5-5	-0.450	4.321	23.177	-0.0001	0.030	1.537	0.072	0.949	2.056
22	n-10-5-5	-0.330	3.664	17.025	0.0000	0.025	1.299	0.062	0.964	1.291
23	n-15-5-5	-0.238	3.512	12.311	0.0003	0.024	1.266	0.057	0.966	1.253
24	n-20-5-5	-0.318	3.077	16.407	-0.0004	0.021	1.082	0.059	0.972	1.119
25	n-5-10-5	-0.420	3.813	21.648	0.0001	0.026	1.330	0.069	0.958	1.562
26	n-5-15-5	-0.135	2.988	7.125	0.0007	0.020	1.048	0.053	0.974	0.964
27	n-5-20-5	-0.328	3.266	16.887	-0.0004	0.022	1.137	0.059	0.970	1.244
28	n-5-5-10	-0.163	3.733	8.605	0.0011	0.025	1.298	0.065	0.964	1.908
29	n-5-5-15	-0.358	3.832	18.454	0.0000	0.026	1.374	0.064	0.957	1.481
30	n-5-5-20	-0.384	3.921	19.811	0.0001	0.026	1.376	0.069	0.960	1.618
31	n-10-10-5	-0.167	3.196	8.735	0.0006	0.022	1.118	0.055	0.971	1.081
32	n-10-15-5	-0.164	3.284	8.565	0.0004	0.022	1.157	0.058	0.969	0.988
33	n-10-20-5	-0.378	3.408	19.523	-0.0002	0.023	1.196	0.063	0.968	1.299
34	n-10-5-10	-0.240	3.443	12.396	0.0002	0.024	1.235	0.057	0.967	1.122
35	n-10-5-15	-0.176	3.156	9.137	0.0005	0.022	1.135	0.054	0.971	1.022
36	n-10-5-20	-0.236	3.265	12.190	-0.0001	0.022	1.152	0.061	0.970	0.873
37	n-10-10-10	-0.245	2.987	12.639	0.0001	0.020	1.039	0.054	0.973	0.627
38	n-10-10-15	-0.285	3.099	14.712	-0.0003	0.021	1.102	0.055	0.970	1.047
39	n-10-10-20	-0.230	2.933	11.915	0.0003	0.020	1.027	0.058	0.973	0.754
40	n-10-15-10	-0.270	3.145	13.989	-0.0001	0.021	1.101	0.058	0.972	0.872
41	n-10-15-15	-0.301	2.986	15.526	-0.0002	0.020	1.054	0.055	0.973	0.884
42	n-10-15-20	-0.272	2.835	14.086	-0.0002	0.019	0.992	0.057	0.974	0.667
43	n-10-20-10	-0.212	3.088	11.010	0.0002	0.021	1.100	0.055	0.972	0.815
44	n-10-20-15	-0.326	2.959	16.867	-0.0004	0.020	1.032	0.059	0.973	1.060
45	n-10-20-20	0.195	2.923	10.098	0.0000	0.020	1.043	0.051	0.974	0.521
46	n-15-5-10	-0.109	3.132	5.871	0.0007	0.022	1.118	0.055	0.971	1.040
47	n-15-5-15	-0.207	3.203	10.714	0.0003	0.022	1.145	0.055	0.970	0.952
48	n-15-5-20	-0.274	3.342	14.175	0.0004	0.023	1.173	0.060	0.968	1.226
49	n-15-10-5	0.089	2.756	4.811	-0.0005	0.019	0.991	0.050	0.975	0.612
50	n-15-10-10	-0.278	3.116	14.317	-0.0002	0.022	1.127	0.053	0.972	0.923
51	n-15-10-15	-0.275	3.174	14.179	-0.0001	0.022	1.136	0.057	0.970	0.917
52	n-15-10-20	0.080	2.720	4.372	-0.0005	0.019	0.973	0.051	0.976	0.502
53	n-15-15-5	-0.305	3.192	15.787	-0.0002	0.021	1.106	0.059	0.971	1.015
54	n-15-15-10	-0.237	2.852	12.240	-0.0003	0.020	1.018	0.053	0.975	0.780
55	n-15-15-15	-0.079	2.927	4.411	0.0005	0.019	1.005	0.062	0.973	0.596
56	n-15-15-20	-0.261	2.894	13.463	-0.0004	0.020	1.035	0.053	0.973	0.877
57	n-20-5-10	-0.170	3.199	8.855	0.0005	0.022	1.133	0.055	0.970	1.000
58	n-20-5-15	-0.162	2.760	8.448	0.0000	0.019	0.987	0.048	0.978	0.330
59	n-20-5-20	-0.078	2.804	4.333	0.0008	0.019	1.001	0.049	0.976	0.860
60	n-20-10-5	-0.004	3.019	1.597	0.0012	0.020	1.058	0.054	0.973	1.206
61	n-20-10-10	-0.094	3.092	5.109	0.0004	0.021	1.093	0.055	0.971	0.741
62	n-20-10-15	-0.320	3.004	16.516	-0.0005	0.020	1.062	0.056	0.972	1.158
63	n-20-10-20	-0.146	2.775	7.634	0.0000	0.019	0.973	0.055	0.976	0.297
64	n-20-15-5	-0.156	3.139	8.165	0.0006	0.022	1.133	0.055	0.971	1.119
65	n-20-15-10	-0.250	2.886	12.935	0.0001	0.020	1.015	0.056	0.975	0.629
66	n-20-15-15	-0.187	2.913	9.731	-0.0001	0.020	1.019	0.061	0.974	0.497
67	n-20-15-20	-0.179	2.761	9.283	-0.0001	0.019	0.994	0.049	0.975	0.438
68	n-20-20-5	-0.207	3.010	10.743	0.0001	0.020	1.065	0.054	0.973	0.615
69	n-20-20-10	-0.219	3.058	11.339	0.0000	0.021	1.096	0.052	0.972	0.637
70	n-20-20-15	-0.065	2.735	3.679	0.0005	0.019	0.981	0.049	0.976	0.525
71	n-20-20-20	0.046	2.755	2.769	0.0009	0.019	0.965	0.057	0.975	0.822



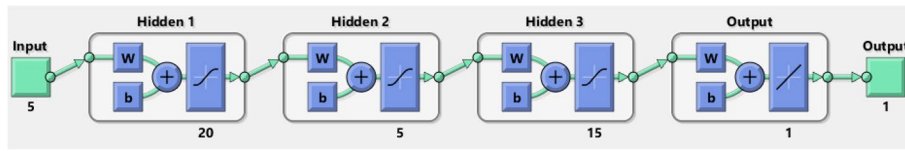


**Fig. 1** Structure of the trained slug liquid holdup ANN model

$$E_{rms} = \sqrt{\frac{1}{n} \left( \sum_{i=1}^n e_{ri}^2 \right)} \tag{6}$$

$$R = \sqrt{1 - \left( \frac{\sum_{i=1}^n e_i}{\sum_{i=1}^n \bar{e}_{imeas}} \right)} \tag{7}$$

$$e_{ri} = \frac{H_{LSi_{pred}} - H_{LSi_{meas}}}{H_{LSi_{meas}}} \tag{8}$$

$$e_i = H_{LSi_{pred}} - H_{LSi_{meas}} \tag{9}$$

$$E_1 = \frac{1}{n} \left( \sum_{i=1}^n e_{ri} \right) \tag{10}$$

$$E_2 = \frac{1}{n} \left( \sum_{i=1}^n |e_{ri}| \right) \tag{11}$$

$$E_3 = \sum_{i=1}^n \sqrt{\frac{(e_{ri} - E_1)^2}{n - 1}} \tag{12}$$

$$E_4 = \frac{1}{n} \left( \sum_{i=1}^n e_i \right) \tag{13}$$

$$E_5 = \frac{1}{n} \left( \sum_{i=1}^n |e_i| \right) \tag{14}$$

$$E_6 = \sum_{i=1}^n \sqrt{\frac{(e_i - E_4)^2}{n - 1}} \tag{15}$$

$$\bar{e}_{imeas} = H_{LSi_{meas}} - \bar{H}_{LSi_{meas}} \tag{16}$$

$$\bar{H}_{LSi_{meas}} = \frac{1}{n} \left( \sum_{i=1}^n H_{LSi_{meas}} \right) \tag{17}$$

where  $e_{ri}$  is the relative error,  $e_i$  is the actual error,  $E_1$  is the average percent error,  $E_2$  is the absolute average percent error,  $E_3$  is the percent standard deviation,  $E_4$  is the average



error,  $E_5$  is the absolute average error,  $E_6$  is the standard deviation,  $\bar{e}_{imeas}$  is the average change in measured SLH,  $\bar{H}_{LS_{meas}}$  is average measured slug liquid holdup,  $H_{LSi_{meas}}$  is measured liquid holdup,  $H_{LSi_{pred}}$  is the predicted liquid holdup, R is the correlation coefficient,  $E_{rms}$  is the root-mean-square error, and  $F_{rp}$  is a relative performance factor.

**Slug liquid holdup ANN visible mathematical model development**

The SLH-ANN-BBM developed in the “Slug liquid holdup ANN black-box model development” section was presented without any visible mathematical equation. This will make it difficult for readers to implement the developed ANN model. There is therefore the need for a translation of the SLH-ANN-BBM into a SLH-ANN-VMM with the aid of the extracted weights and biases and the activation functions.

As already mentioned, the trained optimum ANN consist of 3 HLs with 20 neurons in the first HL, 5 neurons in the second HL, and 15 neurons in the third HL. From here, we will refer to the input layer as the first layer, first HL as second layer, second HL as third layer, third HL as fourth layer, and output layer as the fifth layer. The second, third, fourth, and fifth layers extracted biases and weights are as presented in Tables 5, 6, 7, and 8, respectively. The SLH-ANN-VMM development is described next.

First, an input vector Y of seven variables representing the inputs  $V_{SG}$ ,  $V_{SL}$ ,  $\mu_L$ , d,  $\rho_L$ ,  $\theta$ , and  $\sigma_L$  is defined. In the preprocessing step, six out of the seven input variables were transformed to dimensionless numbers:  $N_{GV}$ ,  $N_{LV}$ ,  $N_d$ , and  $N_L$  with the aid of Eqs. (1),

**Table 5** Second layer’s bias vector,  $b^{L2}$ , and weight matrix,  $W^{L2}$ , used in Eq. (19)

$W^{L2}$					$b^{L2}$
$N_{GV}$	$N_{LV}$	$N_d$	$N_L$	$\theta$	
0.203	0.344	0.321	- 5.572	- 0.490	- 5.062
- 0.065	0.477	- 4.897	- 0.595	- 0.564	- 5.633
- 0.643	0.178	- 0.707	1.448	- 1.479	1.946
- 0.575	3.195	2.099	- 1.192	- 0.341	3.867
- 1.436	2.424	- 0.094	- 0.555	- 0.292	1.569
1.519	- 1.903	0.435	1.574	1.178	- 0.967
- 0.200	- 0.510	- 4.850	1.944	0.177	- 0.317
- 0.353	- 1.191	- 0.733	- 2.984	2.561	0.453
1.324	1.661	0.053	1.409	2.020	- 0.143
- 1.190	- 1.013	- 0.925	- 1.277	0.212	0.101
0.930	1.183	- 0.230	- 1.363	- 1.810	- 0.275
1.533	1.675	- 0.184	- 0.027	2.307	0.607
0.145	0.053	- 3.344	- 1.675	0.133	- 0.243
0.268	1.108	1.692	- 1.394	1.964	- 1.273
- 0.978	1.130	0.179	- 1.090	- 0.895	- 1.489
1.151	1.345	1.067	0.475	- 0.666	1.225
0.174	- 0.298	0.075	2.520	- 4.354	- 2.882
0.238	- 0.633	2.813	0.402	1.299	1.853
0.218	- 2.118	0.963	- 1.441	1.563	1.462
2.615	- 0.424	- 0.161	- 0.631	- 0.386	2.685

**Table 6** Third layer's bias vector,  $b^3$ , and weight matrix,  $w^3$ , used in Eq. (21)

$w^3$												$b^3$								
-0.103	0.102	0.655	0.148	0.141	0.319	-0.552	0.901	0.226	0.406	-0.598	-0.382	0.887	0.770	0.241	0.282	1.013	-0.613	0.276	0.354	-2.406
-1.048	0.888	0.788	0.119	-0.502	0.763	-0.021	-1.853	0.025	-1.539	2.420	-0.768	1.442	0.009	-0.061	0.320	-0.969	1.597	0.208	0.648	-0.126
-6.317	2.835	1.733	2.220	-0.055	-1.739	-2.399	-0.810	0.307	0.791	0.369	-0.038	-1.890	0.145	-0.373	0.541	0.852	-1.612	0.496	-0.173	1.092
-0.480	0.845	0.072	-0.022	-0.220	-0.538	-0.673	0.324	0.138	-0.978	-0.179	-0.746	1.222	-0.030	0.289	0.406	0.585	-0.136	0.562	-0.303	-0.969
-0.182	3.298	0.621	-1.733	0.422	0.445	-0.625	-0.916	-0.835	0.395	0.751	-0.754	1.183	1.312	-0.893	-0.118	-1.422	1.573	0.672	1.270	-0.901

**Table 7** Fourth layer’s bias vector,  $b^{L4}$ , and weight matrix,  $W^{L4}$ , used in Eq. (23)

$W^{L4}$					$b^{L4}$
-0.914	0.563	1.956	1.416	2.873	2.417
-0.611	-1.582	-2.605	-0.661	2.217	2.748
-1.464	-1.482	0.005	-1.118	0.167	1.589
1.631	0.884	-0.761	0.415	0.999	-1.527
-1.741	0.014	1.376	0.064	-1.330	1.150
1.422	-1.787	1.919	0.856	2.005	-1.344
-1.375	0.799	-5.227	0.564	1.149	-0.730
0.637	1.800	2.138	-1.029	0.106	-1.878
-0.615	1.833	-0.095	-1.141	-1.365	-0.100
0.061	-2.533	0.204	-0.349	-1.886	0.040
2.171	0.978	-2.516	2.134	0.979	2.019
1.958	2.343	2.617	-1.440	0.501	0.909
-1.842	2.183	1.928	0.474	0.485	-2.205
0.668	1.977	-0.276	0.423	2.322	1.264
1.202	1.550	1.803	-1.538	-0.758	2.649

(2), (3), and (4), respectively. Similarly, in developing the ANN-VMM, the dataset is transformed to dimensionless numbers with the aid of Eqs. (1), (2), (3), and (4).

Second, the dimensionless numbers ( $N_{GV}$ ,  $N_{LV}$ ,  $N_d$ , and  $N_L$ ) and the angle of inclination,  $\theta$ , were used as inputs in the training of the ANN. Hence, an input vector  $X$  of five variables:  $X_1$ ,  $X_2$ ,  $X_3$ ,  $X_4$ , and  $X_5$  representing the inputs  $N_{GV}$ ,  $N_{LV}$ ,  $N_d$ ,  $N_L$ , and  $\theta$  is defined. Before training of the ANN, the default feed forward network processing function as given in Eq. (18) was used to normalize the inputs to lie between  $-1$  and  $+1$ .

$$a^{L1} = X_{n(-1:1)} = 2 \left[ \frac{X - X_{min}}{X_{max} - X_{min}} \right] - 1 \tag{18}$$

where  $X_{(-1:1)}$  is the input vector normalized in the range  $\{-1, +1\}$ ,  $X_{min}$  is the minimum training dataset input vector as shown in column 4 of Table 3,  $X_{max}$  is the maximum training dataset input vector as shown in column 5 of Table 3, and  $a^{L1}$  is the first layer’s activation vector.

Third, the second layer’s (first HL’s) net input vector,  $Z^{L2}$ , is determined as the sum of second layer’s bias vector,  $b^{L2}$ , and the product of the second layer’s weight matrix,  $W^{L2}$ , and first layer’s activation vector,  $a^{L1}$ , as defined in Eq. (19). Second layer’s bias vector,  $b^{L2}$ , and weight matrix,  $W^{L2}$ , are listed in Table 5.

$$Z^{L2} = b^{L2} + W^{L2} \cdot a^{L1} \tag{19}$$

Fourth, the second layer’s activation vector is determined to lie in the range between  $-1$  and  $+1$  by using Eq. (20), the hyperbolic tangent activation function.

$$a^{L2} = \left( \frac{2}{1 + \exp(-2Z^{L2})} \right) - 1 = \tanh(Z^{L2}) \tag{20}$$

**Table 8** Fifth layer's bias,  $b^{L5}$ , and weight vector,  $w^{L5}$ , used in Eq. (25)

$w^{L5}$											$b^{L5}$				
0.757	-0.424	-0.418	0.486	0.637	1.142	-0.381	-1.564	1.274	-0.921	-0.918	-0.789	0.972	-1.154	-1.004	0.526

Fifth, the third layer's (second HL's) net input vector,  $Z^{L3}$ , is determined as the sum of the third layer's bias vector,  $b^{L3}$ , and the product of the third layer's weight matrix,  $W^{L3}$ , and the second layer's activation vector,  $a^{L2}$ , as expressed in Eq. (21). Third layer's bias vector,  $b^{L3}$ , and weight matrix,  $W^{L3}$ , are listed in Table 6.

$$Z^{L3} = b^{L3} + W^{L3} \cdot a^{L2} \tag{21}$$

Sixth, the third layer's activation vector is computed to lie in the range  $\{-1, +1\}$  with the aid of Eq. (22), the hyperbolic tangent activation function.

$$a^{L3} = \left( \frac{2}{1 + \exp(-2Z^{L3})} \right) - 1 = \tanh(Z^{L3}) \tag{22}$$

Seventh, the fourth layer's (third HL's) net input vector,  $Z^{L4}$ , is determined as the sum of the fourth layer's bias vector,  $b^{L4}$ , and the product of the fourth layer's weight matrix,  $W^{L4}$ , and the third layer's activation vector,  $a^{L3}$ , as defined in Eq. (23). Fourth layer's bias vector,  $b^{L4}$ , and weight matrix,  $W^{L4}$ , are listed in Table 7.

$$Z^{L4} = b^{L4} + W^{L4} \cdot a^{L3} \tag{23}$$

Eighth, the fourth layer's activation vector is computed to lie in the range  $\{-1, +1\}$  with the aid of Eq. (24), the hyperbolic tangent activation function.

$$a^{L4} = \left( \frac{2}{1 + \exp(-2Z^{L4})} \right) - 1 = \tanh(Z^{L4}) \tag{24}$$

Ninth, the fifth layer's (output layer's) net input,  $Z^{L5}$ , is determined as the sum of the fifth layer's bias,  $b^{L5}$ , and the product of the fifth layer's weight vector,  $W^{L4}$ , and the fourth layer's activation vector,  $a^{L4}$ , as defined in Eq. (25). Fifth layer's bias,  $b^{L5}$ , and weight vector,  $W^{L5}$ , are listed in Table 8.

$$Z^{L5} = b^{L5} + W^{L5} \cdot a^{L4} \tag{25}$$

Tenth, the fifth layer's (output layer's) net input vector,  $Z^{L5}$ , is denormalized with the aid of Eq. (26) to produce the output (slug liquid holdup).

$$H_{LS} = \frac{(Z^{L5} + 1)}{2} (H_{LSmax} - H_{LSmin}) + H_{LSmin} \tag{26}$$

where  $H_{LS}$  is the predicted slug liquid holdup,  $Z^{L5}$  is the fifth layer's (output layer's) net input,  $H_{LSmax}$  is the maximum value of training dataset slug liquid holdup equal to 1.0 as shown in column 5, row 8 of Table 3, and  $H_{LSmin}$  is the minimum value of the training dataset slug liquid holdup equal to 0.164 as shown in column 4, row 8 of Table 3.

The flow chart for predicting of SLH with the proposed SLH-ANN-VMM is as shown in Fig. 2. In addition, a MATLAB code of the proposed SLH-ANN-VMM is presented in Appendix Table 13.

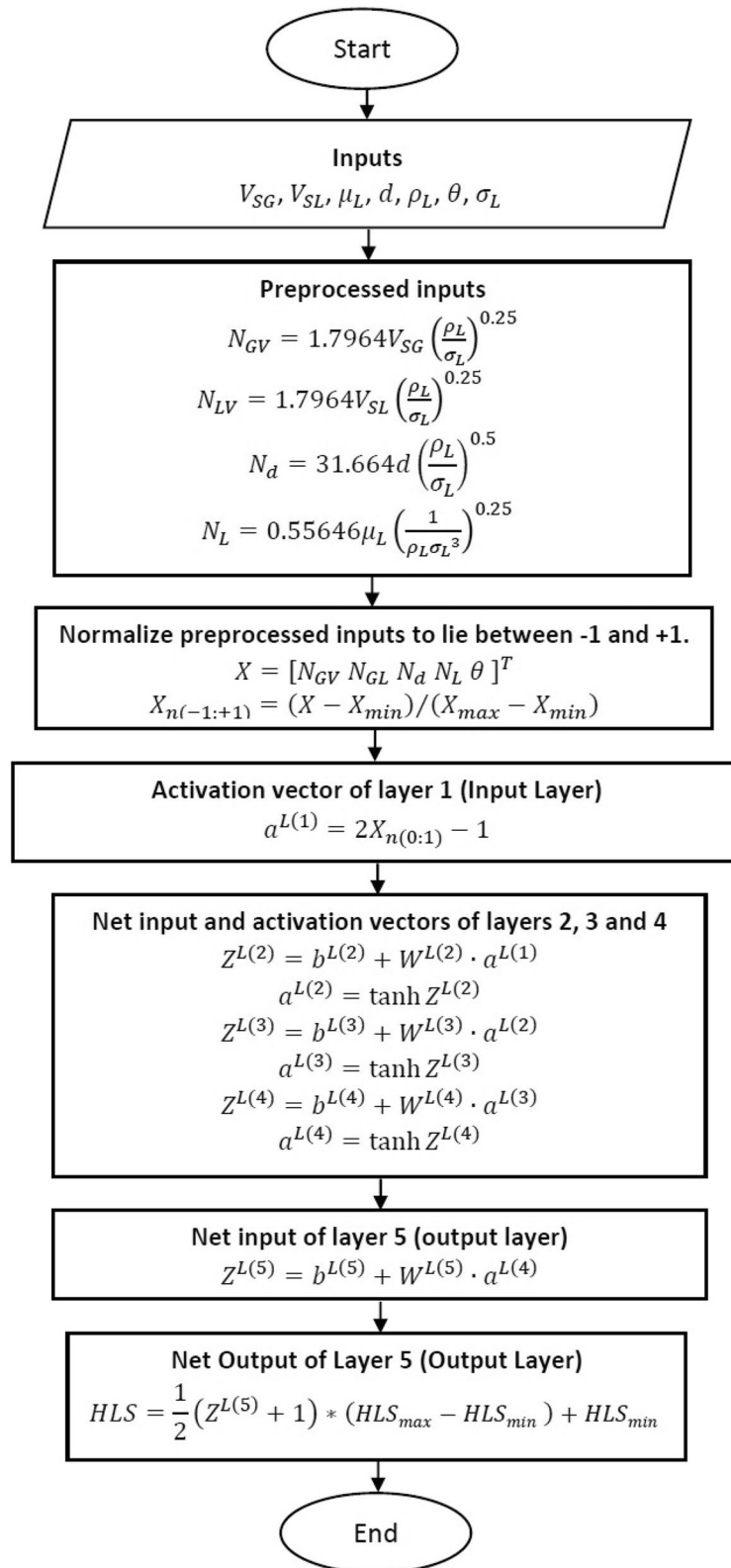


Fig. 2 Flow chart for the predicting of slug liquid holdup with the proposed SLH-ANN-VMM

### Results and discussion

Three important tests were performed to evaluate the proposed SLH-ANN-VMM. These tests include trend analysis, test against measured dataset, and comparison against best available models.

#### Trend analysis of the SLH-ANN-VMM based on synthetic slug flow dataset

We conducted a trend analysis to confirm whether the proposed SLH-ANN-VMM reproduced the expected effect of each input variable on the SLH. First, seven different synthetic datasets were generated. Each synthetic dataset was generated by varying one input and keeping the other inputs constant. The constant inputs used in the synthetic datasets generation are as defined in Table 1, column 6. Second, the proposed SLH-ANN-VMM and the best available SLH-ANN-VMM [30] were used to predict the SLH for each of the seven synthetic datasets. Third, plot of each of the varied input parameter against the SLH is made.

Figure 3 shows the effect of superficial gas velocity (SGV) on slug liquid holdup (SLH). Generally, an increase in SGV results in a decrease in SLH. This is because increasing the

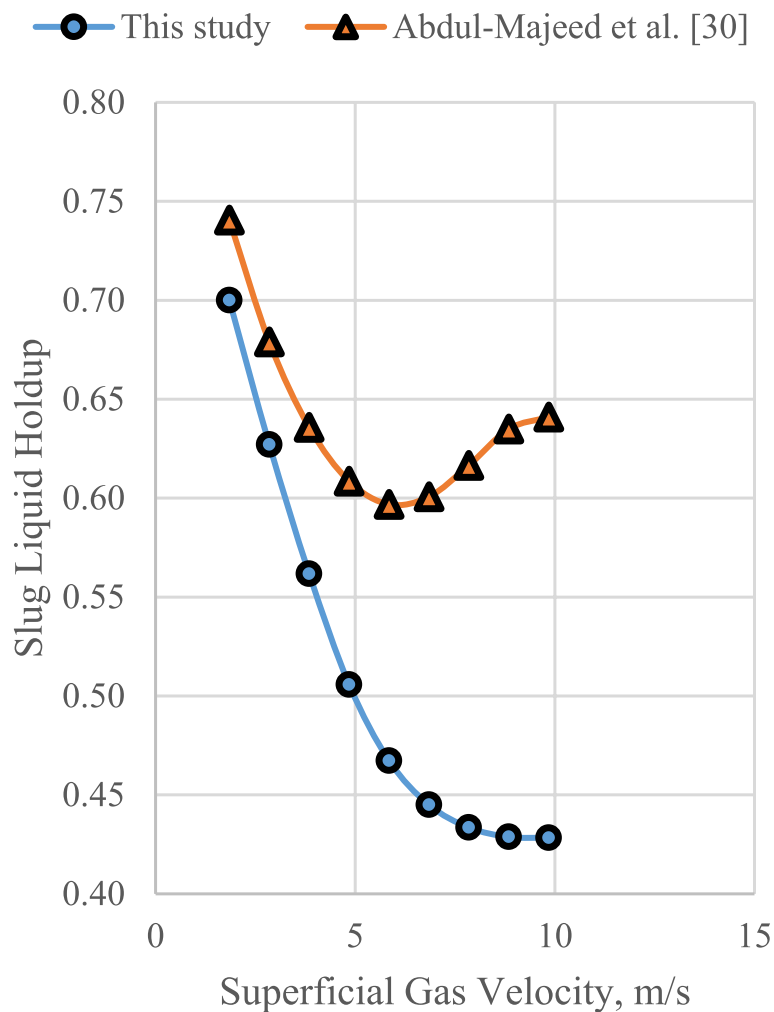


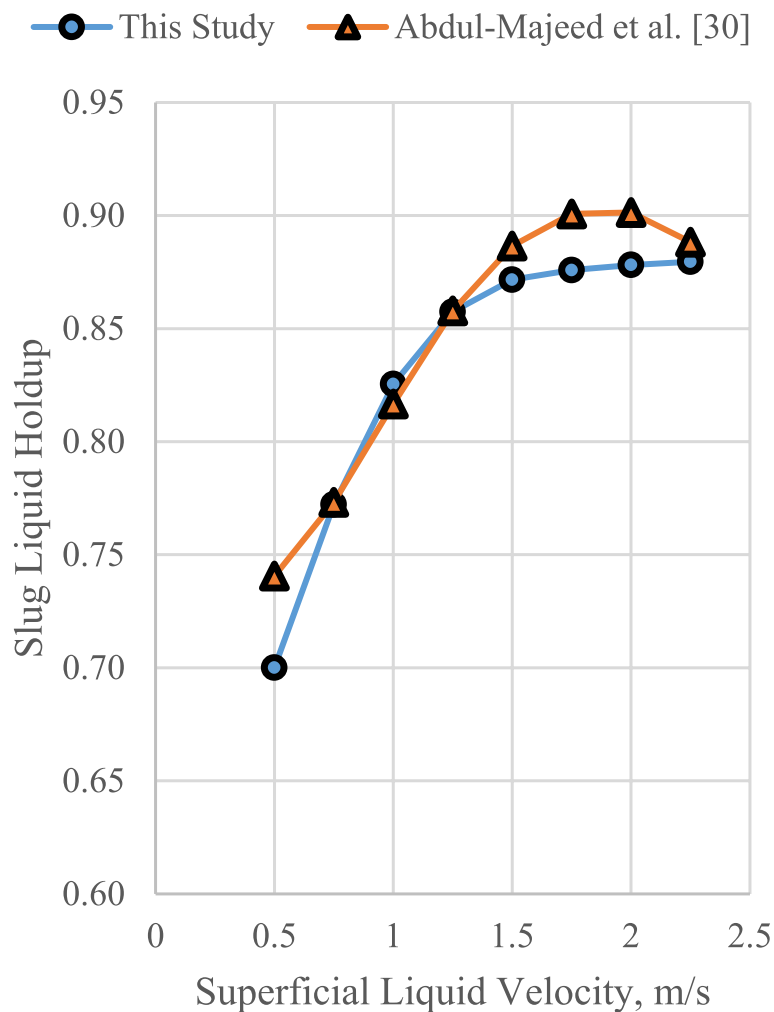
**Fig. 3** Effect of superficial gas velocity on slug liquid holdup



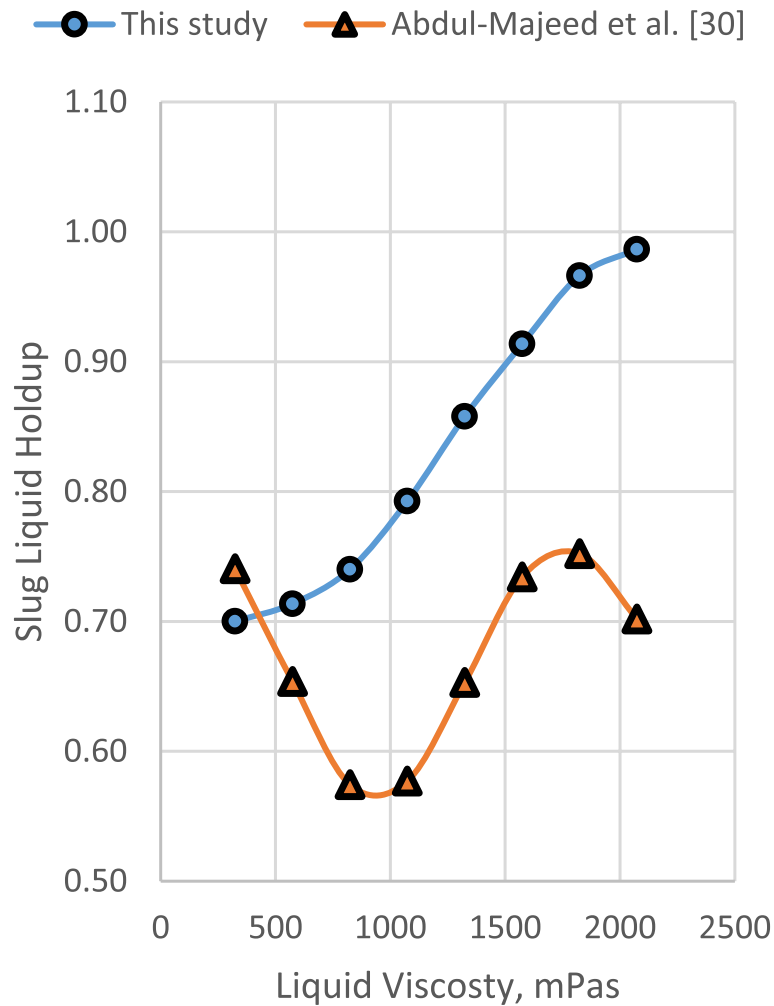
SGV will sweep out most of the liquid phase from the pipe resulting in more of the pipe cross section occupied by the gas phase [45]. This of course will result in an increase in the gas void fraction and a corresponding decrease in the SLH. Hence, as shown in Fig. 3, the proposed SLH-ANN-VMM and Abdul-Majeed et al. SLH-ANN-VMM [30] simulate the expected decrease in SLH with an increase in superficial gas velocity.

Figure 4 shows the effect of superficial liquid velocity (SLV) on SLH. Generally, an increase in SLV results in a slight increase in SLH because of an increase in the pipe’s input liquid content [19]. Hence, as evident in Fig. 4, the proposed SLH-ANN-VMM and Abdul-Majeed et al. SLH-ANN-VMM [30] simulate the expected slight increase in SLH with an increase in SLV.

Figure 5 shows the effect of liquid viscosity (LV) on SLH for medium to high LV. It has been reported in several experimental studies [20, 24, 34, 45] that for medium to high LV, SLH increases with an increase in LV. This is because an increase in LV will increase both the shear around the pipe wall and resistance of liquid flow which will result in an increase in SLH. It is therefore evident from Fig. 5 that for medium to high LV, the proposed SLH-ANN-VMM simulates the expected increase in SLH with an increase in LV.



**Fig. 4** Effect of superficial liquid velocity on slug liquid holdup



**Fig. 5** Effect of liquid viscosity on slug liquid holdup for medium to high liquid viscosity

However, the Abdul-Majeed et al. SLH-ANN-VMM [30] did not simulate the expected effect of LV on SLH.

Figure 6 shows the effect of LV on SLH for low LV. The dual effect of LV on SLH has been reported in several studies [46–48]. These researchers observed that SLH decreased with an increase in LV for LV,  $\mu_L \leq 3\text{mPas}$ , and increased with increase in LV for LV,  $\mu_L > 3\text{mPas}$ . For  $\mu_L \leq 3\text{mPas}$ , the low drag forces contribute to a more uniform bubble distribution which of course results in decrease SLH. For  $\mu_L > 3\text{mPas}$ , the large drag forces contribute to bubble coalescence which results in an increase in SLH. It is evident from Fig. 6 that the proposed SLH-ANN-VMM and Abdul-Majeed et al. SLH-ANN-VMM [30] do not simulate the dual effect of LV on SLH. Instead, SLH was observed to increase slightly with an increase LV for both models which is in agreement with the observations of several authors [46–48] for LV,  $\mu_L > 3\text{mPas}$ .

Figure 7 shows the effect of pipe internal diameter (PID) on SLH. It has been reported in several studies [11, 28, 49, 50] that SLH increases slightly with an increase in PID. This increase in SLH with an increase in PID is because of the increase in bubble rise velocity with an increase in PID [51]. It is evident from Fig. 7 that the proposed SLH-ANN-VMM

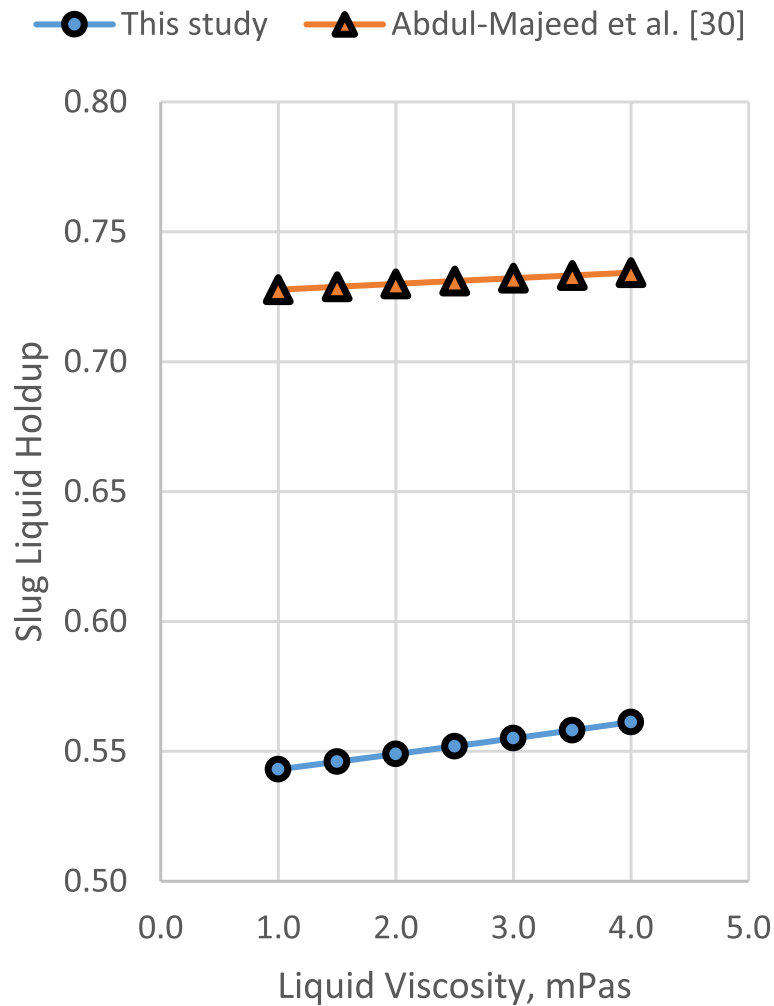


**Fig. 6** Effect of liquid viscosity on slug liquid holdup for low liquid viscosity

simulates the expected increase in SLH with an increase in PID. It is also evident from Fig. 7 that the Abdul-Majeed et al. SLH-ANN-VMM [30] did not simulate the expected increase of SLH with PID.

Figure 8 shows the effect of pipe inclination angle (PIA) on SLH. It has been observed based on experimental data that SLH decreases with an increase in PIA with a maximum value for horizontal flow and minimum for vertical upward flow [33]. This observed decrease in SLH with an increase PIA has been confirmed in some studies [11, 52]. As shown in Fig. 8, the proposed SLH-ANN-VMM and Abdul-Majeed et al. SLH-ANN-VMM [30] simulate the expected decrease in SLH with an increase of PIA up to 30° and 15° respectively.

Figure 9 shows the effect of surface tension (ST) on SLH. It is expected that SLH increases with increase in ST. This is because increase in ST promotes increase in bubble rise velocity which results in an increase in SLH [19]. As evident in Fig. 9, the proposed SLH-ANN-VMM and the Abdul-Majeed et al. SLH-ANN-VMM [30] simulate the expected increase in SLH with increase in ST.

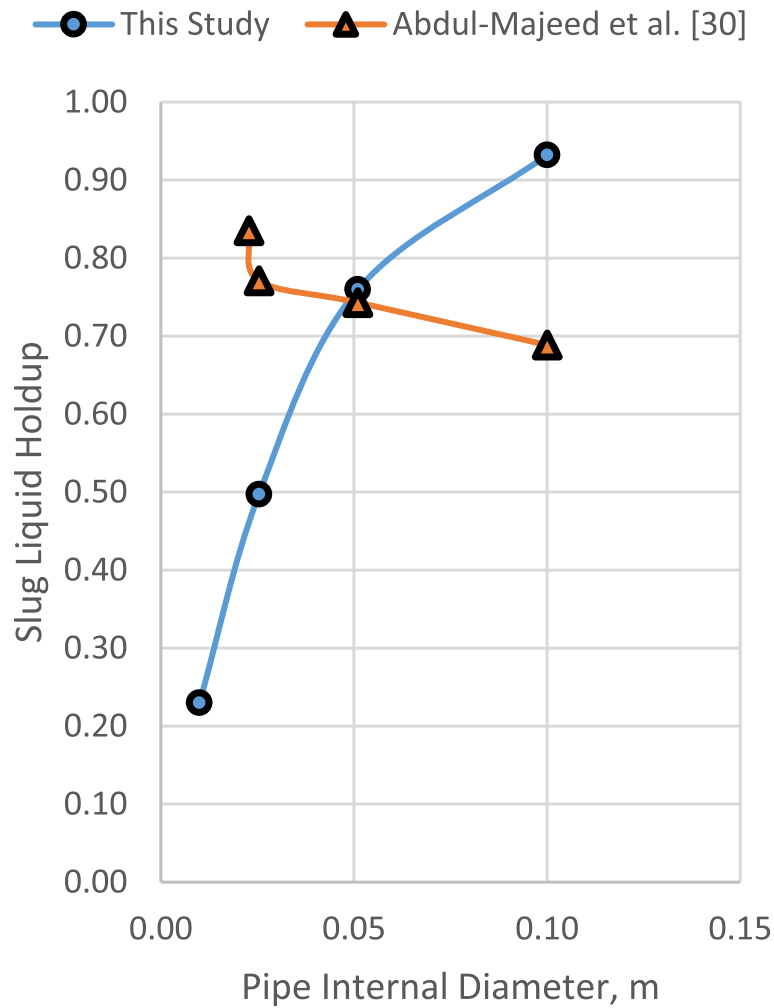


**Fig. 7** Effect of pipe internal diameter on slug liquid holdup

**Test of the SLH-ANN-VMM against measured slug flow dataset**

In this section, we tested the prediction accuracy of the trained optimum network structure against laboratory-measured slug flow dataset. This was done by using the trained optimum network to predict the SLH based on the training, testing, validation, and entire datasets respectively. Next, measured and predicted SLH cross-plots with unit slope and trend lines are used to evaluate the accuracy of the developed model. In addition, the coefficient of determination (*R*-squared) is included in the cross-plot.

We considered the developed model accurate and in agreement with measured dataset if the two conditions are satisfied. First, majority of the cross-plots must be clustered close to the unit slope line. Second, the coefficient of determination must increase in the order of testing, validation, entire, and training datasets.

As shown in Figs. 10, 11, 12, and 13, majority of the cross-plots are clustered close to the unit slope line with a coefficient of determinations of 0.9791, 0.9727, 0.9756, and 0.9776 for training, testing, validation, and entire datasets respectively. Notice that the coefficient of determination increases in the order of testing, validation, entire, and

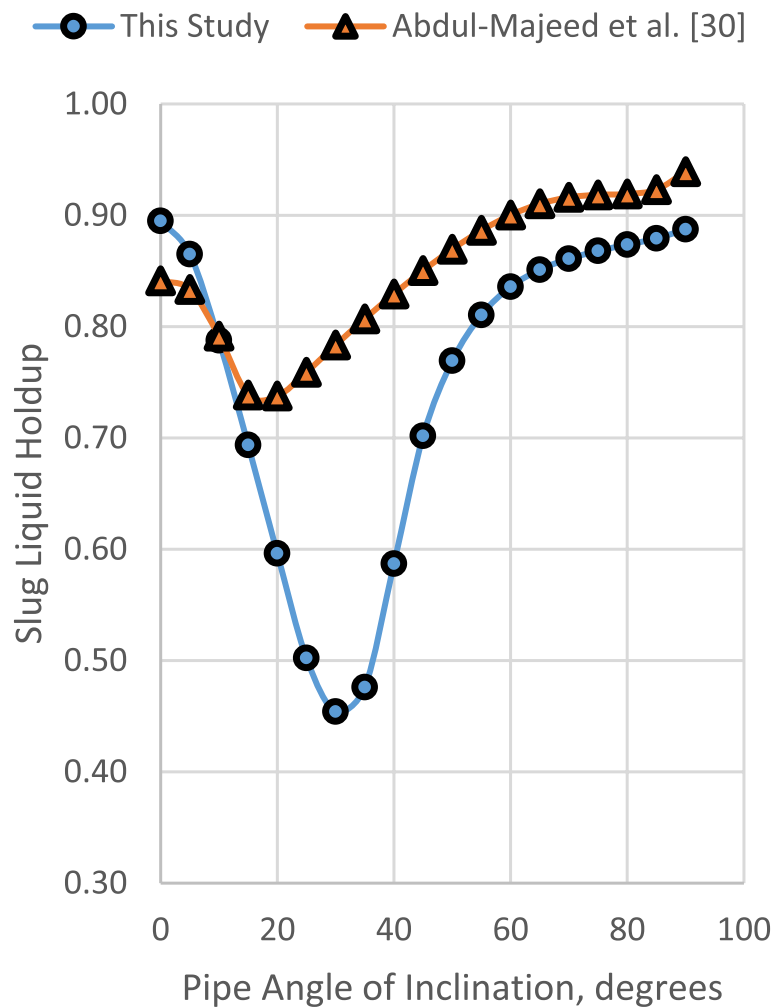


**Fig. 8** Effect of pipe angle of inclination on slug liquid holdup

training datasets. This clearly shows that the two conditions are satisfied, and hence, the proposed SLH-ANN-VMM predictions are in close agreement with measured SLH.

**Comparison of SLH-ANN-VMM against existing correlations and models**

The 2699 laboratory-measured slug flow data points were used for comparing the performance of the present model against that of 8 available SLH correlations [18–21, 23, 24, 31, 34] and 1 machine learning model [30]. Statistical and graphical error analyses were employed for the comparative study.

**Statistical error analysis**

Statistical error analysis was employed in this study in comparing the proposed SLH-ANN-VMM against eight existing SLH correlations and the only existing SLH-ANN-VMM. To demonstrate the robustness of the proposed SLH-ANN-VMM, four different comparative studies were performed. First, the proposed SLH-ANN-VMM was compared against horizontal, vertical, and inclined SLH models based on slug flow dataset measured for horizontal, vertical, and inclined slug flow conditions respectively. Second,

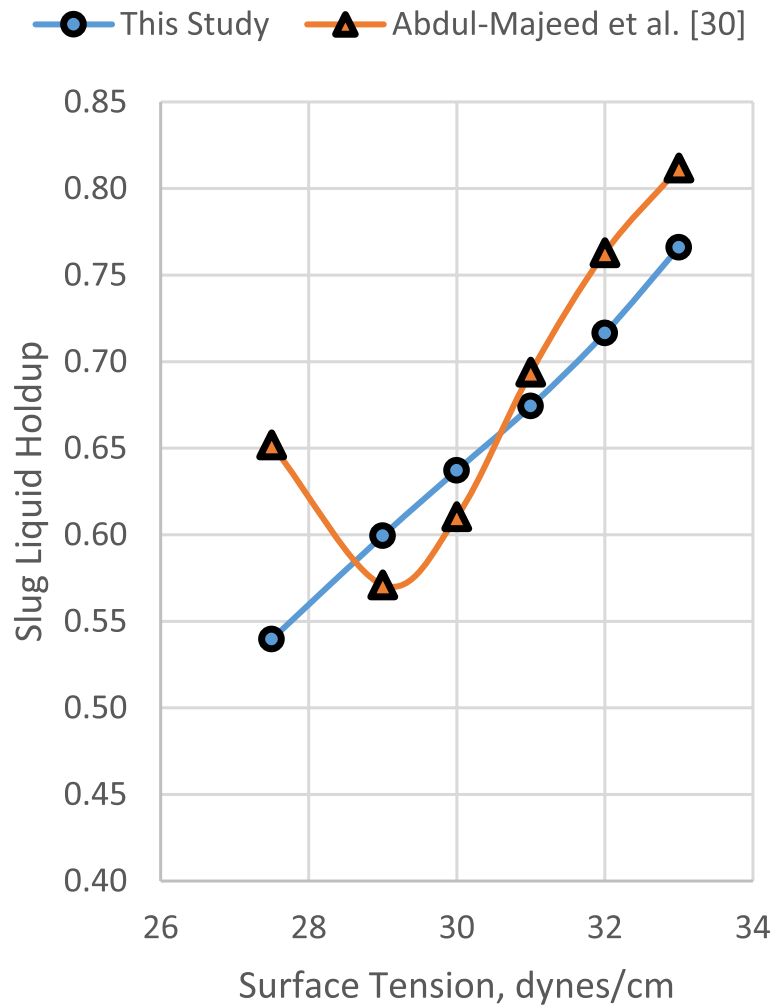


**Fig. 9** Effect of surface tension on slug liquid holdup

the proposed SLH-ANN-VMM was compared against the existing SLH models based on the slug flow dataset measured for horizontal to vertical slug flow conditions.

Relative performance factor,  $F_{rp}$ , as given in Eq. (5) was chosen as the statistical performance indicator for the comparative study because it includes the effect of six statistical errors ( $E_1, E_2, E_3, E_4, E_5,$  and  $E_6$ ) given in Eq. (10) through (15). Relative performance factor,  $F_{rp}$ , ranges from 0 to 6 for best and worst performance respectively.

Tables 9, 10, and 11 summarized the results of the statistical-based comparative performance analysis for the proposed SLH-ANN-VMM and existing horizontal, vertical, and inclined SLH models based slug flow dataset measured for horizontal, vertical, and inclined slug flow conditions respectively. Table 12 summarizes the results of the statistical-based comparative performance analysis for the proposed SLH-ANN-VMM, eight existing SLH correlations, and the only existing SLH-ANN-VMM.

The different models are defined in column 2, while the statistical error parameters,  $E_1$ , through  $E_6$  are defined in columns 3 through 8. Relative performance factor,  $F_{rp}$ , is defined in column 9 for Tables 9, 10, 11, 12. The cells in blue represent the lowest values of each of the six statistical error parameters and the relative performance factor.

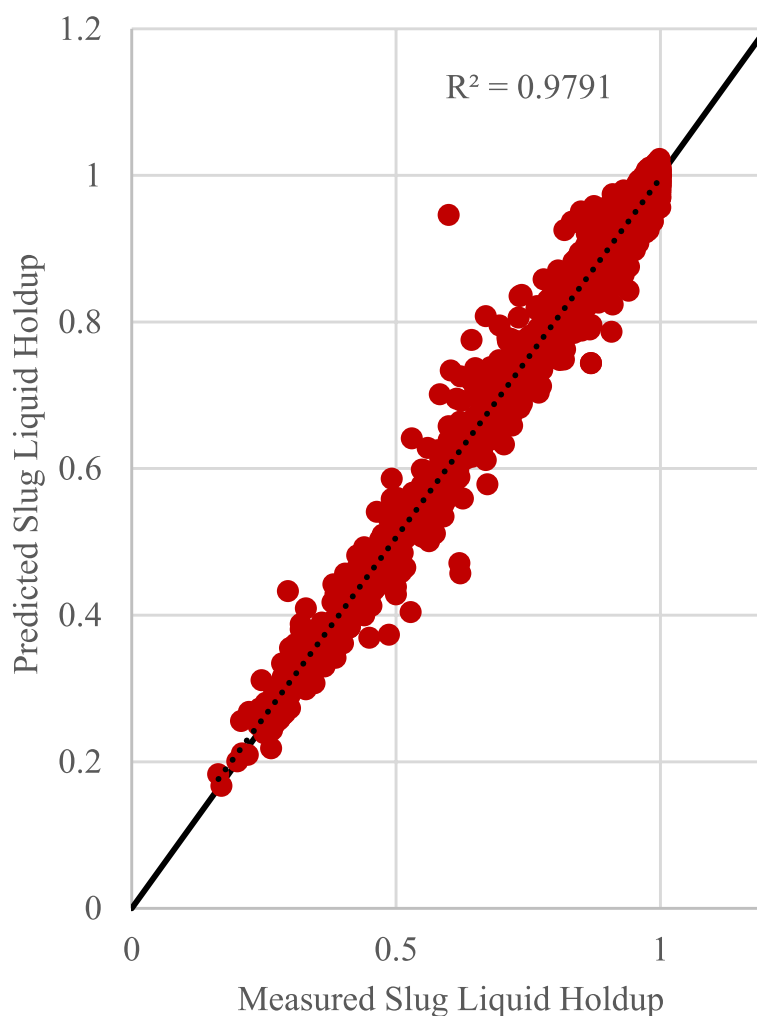


**Fig. 10** Measured and predicted SLH cross-plots for the training dataset (1889 data points)

Furthermore, the models are arranged for convenience in order of increasing the relative performance factor. As already mentioned, relative performance factor,  $F_{rp}$ , was chosen as the statistical performance indicator for the comparative study because it incorporates the effects of  $E_1$ ,  $E_2$ ,  $E_3$ ,  $E_4$ ,  $E_5$ , and  $E_6$ . The best-performing model must achieve the minimum of value of  $F_{rp}$ , while the worst performing must achieve the maximum value of  $F_{rp}$ .

As presented in Tables 9, 10, and 11, this study's SLH-ANN-VMM outperformed existing horizontal, vertical, and inclined SLH models with minimum  $F_{rp}$  of 0.000, 0.000, and 0.006, respectively. Overall as evident in Table 12, this study's SLH-ANN-VMM achieved the best performance with minimum  $F_{rp}$  of 0.002, while the Abdul-Majeed (2000) model achieved the worst performance with maximum  $F_{rp}$  of 5.060.

The performance of the SLH models decreases in the order of this study's SLH-ANN-VMM, Abdul-Majeed et al. [30], Abdul-Majeed and Al-Mashat [19], Sylvester [31], Gregory et al. [23], Kora et al. [24], Archibong-Eso et al. [21], Al-Safran et al. [20], Al-Ruhaimani et al. [34], and Abdul-Majeed [18] models, respectively.



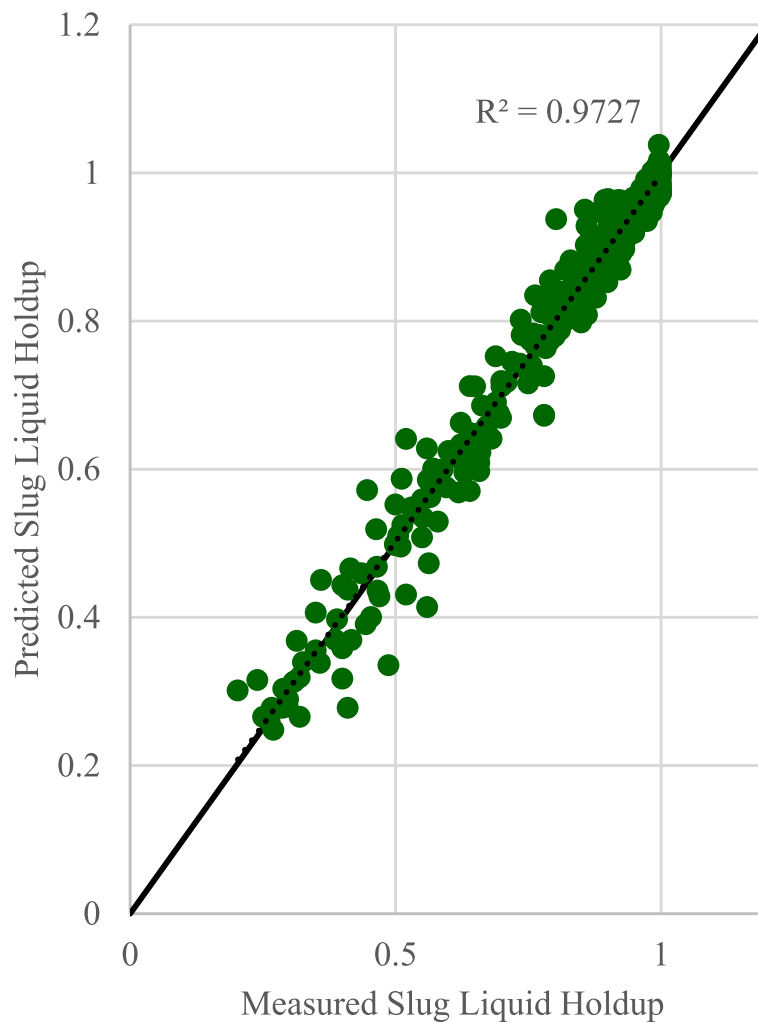


**Fig. 11** Measured and predicted SLH cross-plots for the testing dataset (405 data points)

### Graphical error analysis

*Cross-plots* Figure 14 shows the cross-plots of the measured SLH and predicted SLH by the proposed SLH-ANN-VMM, the eight existing SLH correlations, and an existing SLH-ANN-VMM. First, we constructed the cross-plots of the measured SLH against the SLH predicted by each of the considered models. Second, unit slope line representing a line of perfect correlation is included in the plot. Third, deviation lines of +20% and –20% are included to represent lines of model overprediction and underprediction respectively. We will consider a model to be best performing if majority of its cross-plots are (1) clustered in very close proximity to the unit slope line and (2) within the +20% and –20% deviation lines.

As shown in Fig. 14, the proposed SLH-ANN-VMM have the majority of its cross-plots clustered in very close proximity to the unit slope line and within the +20% and –20% deviation lines. This a clear indication that the proposed SLH-ANN-VMM

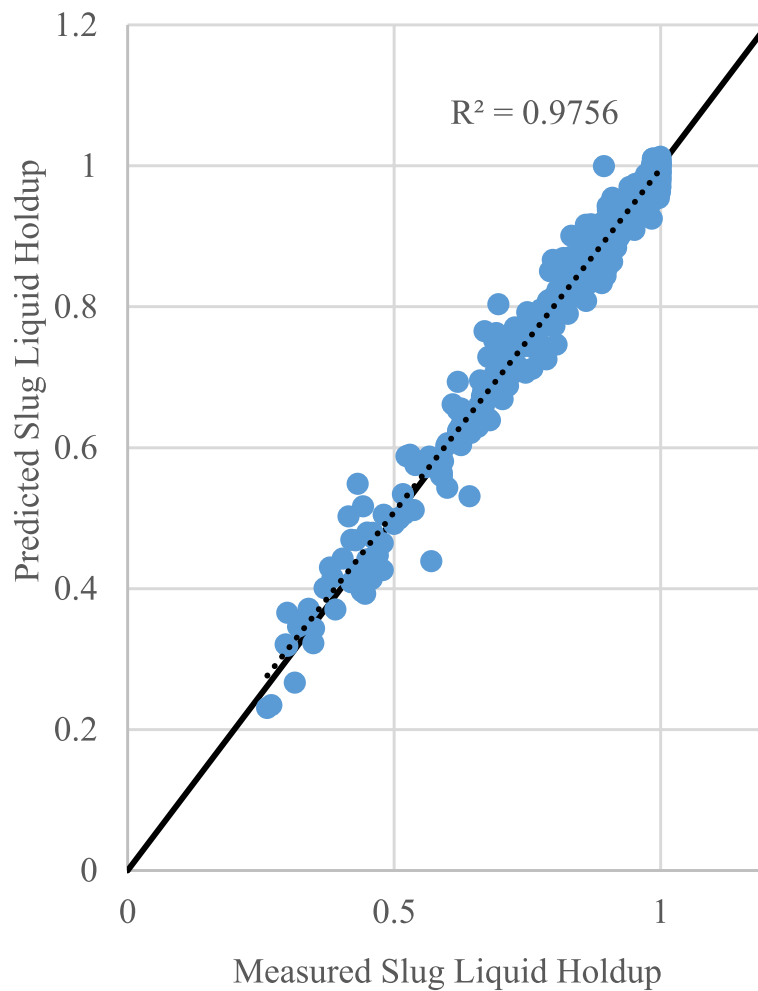


**Fig. 12** Measured and predicted SLH cross-plots for the validation dataset (405 data points)

achieved the best performance. The Abdul-Majeed et al. SLH-ANN-VMM [30] achieved the second best performance with the second highest number of cross-plots clustered in very close proximity in the unit slope line and within the +20% and –20% deviation lines. The Abdul-Majeed correlation [18] achieved the worst performance since only very few of the cross-plots are clustered in close proximity to the unit slope line and within the +20% and –20% deviation lines.

As shown in Fig. 14, we observed that the Abdul-Majeed and Al-Mashat correlation [19] produced negative values of SLH for some data points measured for low viscosity horizontal to near-horizontal flow conditions. These negative values of SLH are because we applied their correlation to flow conditions different from those used in its formulation. Note that the Abdul-Majeed and Al-Mashat correlation [19] was developed with data measured for high viscosity horizontal to vertical upward flow conditions. This a clear prove that these correlations fail when applied to flow conditions different from those used in their formulation.

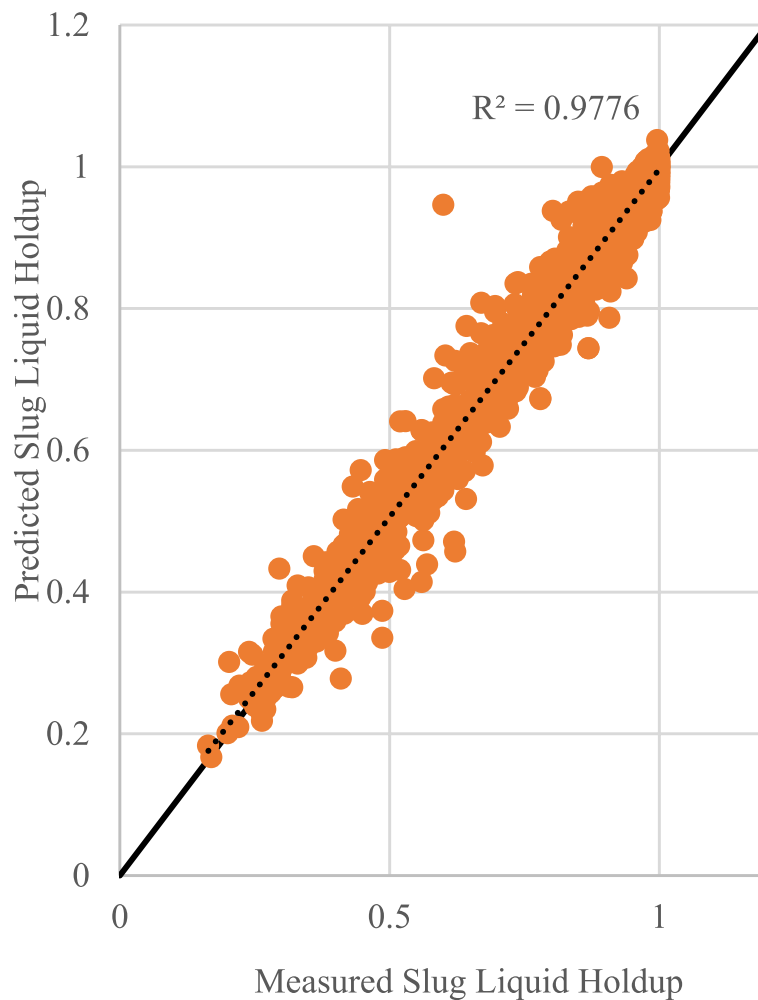


**Fig. 13** Measured and predicted SLH cross-plots for the entire dataset (2669 data points)

*Residual plots* Figure 15 shows the residual plots of the proposed SLH-ANN-VMM, eight existing SLH correlations, and an existing SLH-ANN-VMM. We constructed the residual plots by plotting the number of data point against the actual error (Eq. (9)) achieved by each of the considered model.

Second, a zero actual error line is included to represent a perfect agreement between the measured SLH and SLH predicted by the considered models. Third,  $+0.1$  and  $-0.1$  actual error lines are also included to represent lines of model overprediction and underprediction, respectively. We considered a model to be best performing if majority of the residual plots are (1) clustered in close proximity to the zero actual error line and (2) within the  $+0.1$  and  $-0.1$  actual error lines.

As shown in Fig. 15, the proposed SLH-ANN-VMM achieved the best performance with the majority of the residual plot points clustered in very close proximity to the zero actual error line and within the  $+0.1$  and  $-0.1$  actual error lines. The Abdul-Majeed et al. SLH-ANN-VMM [30] achieved the second best performance with the second highest number of residual plots clustered in very close proximity to the zero

**Table 9** Statistical-based comparative performance analysis for the proposed SLH-ANN-VMM and 7 existing horizontal SLH models based on laboratory-measured horizontal slug flow dataset (1413 data points) [18–21, 23, 24, 30]

S/N	Horizontal Slug Liquid Holdup Models	$E_1$ (%)	$E_2$ (%)	$E_3$ (%)	$E_4$ (-)	$E_5$ (-)	$E_6$ (-)	$F_{TP}$ (-)
1	This Study's SLH-ANN-VMM	0.052	2.652	2.109	0.001	0.020	0.753	0.000
2	Abdul-Majeed et al. [30]	-0.681	4.351	25.337	-0.002	0.032	1.213	0.427
3	Gregory et al. [23]	-4.619	10.003	171.935	-0.018	0.064	2.553	2.035
4	Abdul-Majeed & Al-Mashat [19]	8.363	17.938	311.333	0.054	0.114	4.105	4.209
5	Kora et al. [24]	-16.006	17.709	595.857	-0.086	0.102	4.000	5.265
6	Al-Safran et al. [20]	-16.274	17.905	605.835	-0.088	0.103	4.014	5.337
7	Archibong-Eso et al. [21]	-16.797	17.691	625.305	-0.094	0.103	3.847	5.410
8	Abdul-Majeed [18]	-17.532	20.490	652.666	-0.089	0.118	4.564	5.948

**Table 10** Statistical-based comparative performance analysis for the proposed SLH-ANN-VMM and 4 existing vertical SLH models based on laboratory-measured vertical slug flow dataset (260 data points) [19, 30, 31, 34]

S/N	Vertical Slug Liquid Holdup Model	$E_1$ (%)	$E_2$ (%)	$E_3$ (%)	$E_4$ (%)	$E_5$ (%)	$E_6$ (%)	$F_{rpp}$ (-)
1	This Study's SLH-ANN-VMM	-0.837	4.700	13.391	0.000	0.022	0.353	0.000
2	Abdul-Majeed et al. [30]	-1.182	6.423	18.905	-0.003	0.032	0.519	0.141
3	Abdul-Majeed & Al-Mashat [19]	-36.323	36.491	580.946	-0.141	0.143	2.361	3.262
4	Sylvester [31]	-32.075	50.426	513.014	-0.067	0.239	3.838	3.883
5	Al-Ruhaimani et al. [34]	-66.622	66.855	1065.559	-0.246	0.248	4.003	6.000

**Table 11** Statistical-based comparative performance analysis for the proposed SLH-ANN-VMIM and 3 existing inclined SLH models based on laboratory-measured inclined slug flow dataset (1026 data points) [18, 19, 30]

S/N	Inclined Slug Flow Models	$E_1$ (%)	$E_2$ (%)	$E_3$ (%)	$E_4$ (-)	$E_5$ (-)	$E_6$ (-)	$F_{rp}$ (-)
1	This Study's SLH-ANN-VMIM	-0.287	2.417	9.133	-0.001	0.017	0.542	0.006
2	Abdul-Majeed et al. [30]	-0.511	4.349	16.246	0.000	0.030	0.960	0.097
3	Abdul-Majeed & Al-Mashat [19]	-0.445	15.852	15.058	0.000	0.098	3.152	0.469
4	Abdul-Majeed [18]	16.771	78.962	532.075	0.174	0.644	18.845	6.000

**Table 12** Statistical-based comparative performance analysis for the proposed SLH-ANN-VMM and 9 existing SLH models based on the laboratory-measured horizontal to vertical slug flow dataset (2669 data points) [18–21, 23, 24, 30, 31, 34]

S/N	Slug Liquid Holdup Model	$E_1$ (%)	$E_2$ (%)	$E_3$ (%)	$E_4$ (-)	$E_5$ (-)	$E_6$ (-)	$F_{rp}$ (-)
1	This Study's SLH-ANN-VMM	-0.162	2.760	8.448	0.000	0.019	0.987	0.002
2	Abdul-Majeed et al. [30]	-0.664	4.549	34.185	-0.001	0.031	1.631	0.177
3	Abdul-Majeed & Al-Mashat [19]	0.710	18.932	37.836	0.015	0.111	5.706	1.140
4	Sylvester [31]	-0.119	22.337	14.944	0.056	0.149	6.799	1.724
5	Gregory et al. [23]	-10.386	14.848	534.294	-0.046	0.084	4.845	2.000
6	Kora et al. [24]	-22.367	23.579	1150.587	-0.110	0.122	6.638	4.016
7	Archibong-Eso et al. [21]	-22.561	23.269	1160.593	-0.116	0.122	6.447	4.062
8	Al-Safran et al. [20]	-22.805	23.969	1173.150	-0.112	0.123	6.683	4.088
9	Al-Ruhaimani et al. [34]	-23.577	26.476	1212.832	-0.107	0.135	7.616	4.260
10	Abdul-Majeed [18]	12.556	43.491	645.925	0.116	0.336	17.989	5.060



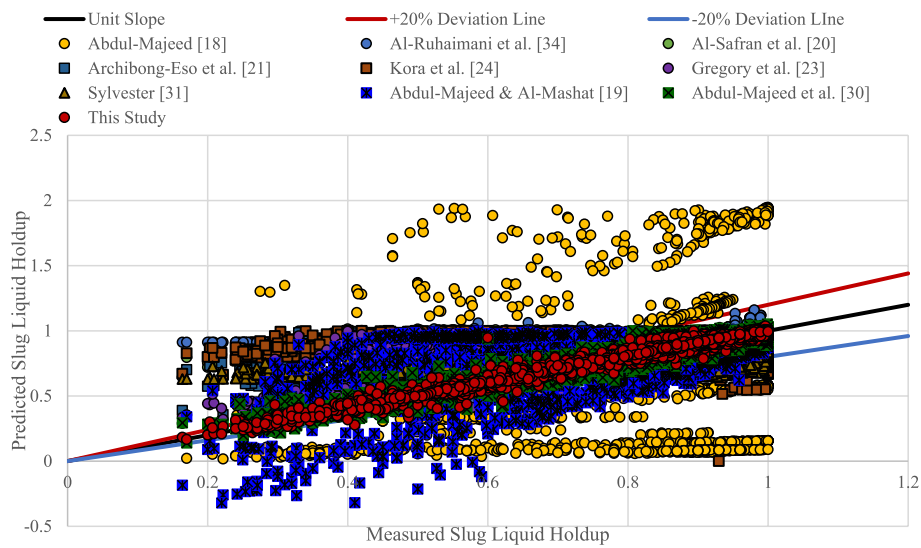


**Fig. 14** Measured SLH and predicted SLH cross-plots for the proposed SLH-ANN-VMM, the eight existing SLH correlations, and an existing SLH-ANN-VMM

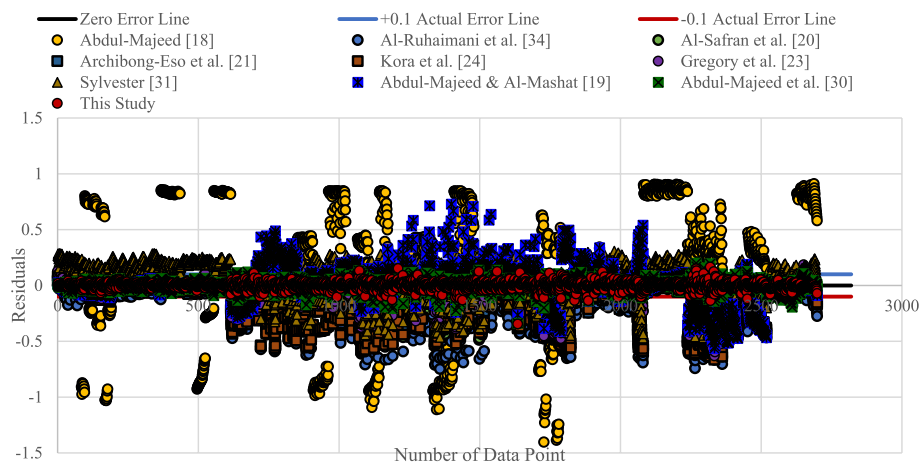


**Fig. 15** Residual plots for the proposed SLH-ANN-VMM, the eight existing SLH correlations, and an existing SLH-ANN-VMM

actual error line and within the + 0.1 and – 0.1 actual error lines. The Abdul-Majeed [18] achieved the worst performance since only very few of the residual plots are clustered in very close proximity to the unit slope line and within the + 0.1 and – 0.1 actual error lines.

This study’s SLH-ANN-VMM outperformed the existing SLH models for several reasons. First, the ANN model was developed with dataset measured for low to high viscosity horizontal to vertical-upward flow conditions. Second, the model was developed with ANN which is capable of mapping the nonlinearity between the inputs and output better than regression analysis. Lastly, the optimum ANN network structure was obtained by selecting the best-performing network structure from a group of structures constructed with one, two, or three HLs with varying numbers of neurons in each HL.

## Conclusions and recommendations

### Conclusions

This study developed slug liquid holdup artificial neural network visible mathematical model (SLH-ANN-VMM) applicable for low to high viscosity horizontal to vertical upward flow conditions. Openly sourced datasets consisting of 2669 data points were used in the construction of 71 different network structures with each structure having either 1, 2, or 3 HLs with varying number of neurons in each HL. Levenberg–Marquardt optimization algorithm was used in training the network, hyperbolic tangent activation function for activating the HLs, and linear activation function for activating the output layer. Comparative performance analysis revealed that the optimum network structure has 20 neurons in the first HL, 5 neurons in the second HL, and 15 neurons in the third HL. The trained SLH-ANN black-box model was translated into a SLH-ANN-VMM with the aid of the extracted biases and weights and the activation functions. Trend analysis revealed that the proposed SLH-ANN-VMM reproduced the expected effects of the various inputs on SLH. Test against measured dataset revealed that the SLHs predicted by the proposed SLH-ANN-VMM are in close agreement with the measured SLHs with the coefficient of determination of 0.9791, 0.9727, 0.9756, and 0.9776 for training, testing, validation, and entire datasets, respectively. Comparative study revealed that the current SLH-ANN-VMM outperformed existing horizontal, vertical, and inclined SLH models with minimum  $F_{rp}$  of 0.000, 0.000, and 0.006, respectively. Comparative study revealed that the proposed SLH-ANN-VMM with a minimum relative performance factor of 0.002 outperformed eight existing SLH empirical correlations and an existing single hidden layered SLH-ANN-VMM.

The findings of this study have added to the existing knowledge in several areas. This study developed an ANN-based model for multiphase SLH prediction for low to high liquid viscosity in horizontal to vertical-upward multiphase pipe flows. The present model was developed and published as visible mathematical equations making its implementation by any user easy and without the need for any ML framework. Unlike existing ANN models that were developed by considering only ANN structures with one hidden layer (HL), the present model was developed by considering ANN structures with one, two, and three HLs. Evaluation results revealed that the developed model predicted SLH better than the best available SLH models and simulated expected effects of inputs on SLH. A user-friendly MATLAB code for SLH prediction is also presented in this study. The code can easily be incorporated into existing mechanistic models for accurate FBHP prediction.

### Recommendations

It is recommended that the proposed SLH-ANN-VMM be used for data points whose parameter ranges are within the minimum and maximum parameter ranges as defined in columns 4 and 5 of Table 1. Slug liquid holdup is one of the critical slug parameters required for accurate prediction of pressure drop during slug flow in pipes. It is therefore recommended that dataset for the other slug flow closure correlations be collected and used to develop an ANN visible mathematical model for the prediction of each of the other slug flow closure correlations.

## Appendix

**Table 13 MATLAB code of the proposed SLH-ANN-VMM**

```

% Input vector
X = x;
% Input parameters
VSG = X(1); VSL = X(2); MuL = X(3); ID = X(4);
RhoL = X(5); Theta = X(6); SigmaL = X(7);
% Pre-processing of inputs
NGV = 1.7964*VSG*(9.8067*RhoL/SigmaL)^0.25;
NLV = 1.7964*VSL*(9.8067*RhoL/SigmaL)^0.25;
ND = 31.664*ID*(9.8067*RhoL/SigmaL)^0.5;
NL = 0.55646*MuL*(1/(9.8067*RhoL*SigmaL^3))^0.25;
% Minimum values of preprocessed input parameters
NGVmin = 0.222097046; NLVmin = 0.082145599;
NDmin = 12.28622042; NLmin = 0.002262319;
Thethamin = 0;
% Maximum values of preprocessed input parameters
NGVmax = 0.222097046; NLVmax = 0.082145599;
NDmax = 12.28622042; NLmax = 0.002262319;
Thethamax = 0;
% Maximum and Minimum Values of preprocessed input parameters
HLSmin = 0.164; HLSmax = 1.0;
% Normalization of preprocessed inputs to lie between -1 and +1
NGVn = 2*((NGV-NGVmin)/(NGVmax-NGVmin))-1;
NLVn = 2*((NLV-NLVmin)/(NLVmax-NLVmin))-1;
NDn = 2*((ND-NDmin)/(NDmax-NDmin))-1;
NLn = 2*((NL-NLmin)/(NLmax-NLmin))-1;
Thethan = 2*((Theta-Thethamin)/(Thethamax-Thethamin))-1;
% Activation vector of Layer 1
aL1 = [NGVn NLVn NDn NLn Thethan]';
% Net input and activation vectors of Layer 2
ZL2 = bL2 + WL2*aL1;
aL2 = tanh(ZL2);
% Net input and activation vectors of Layer 3
ZL3 = bL3 + WL3*aL2;
aL3 = tanh(ZL3);
% Net input and activation vectors of Layer 4
ZL4 = bL4 + WL4*aL3;
aL4 = tanh(ZL4);
% Net input vector of Layer 5
ZL5 = bL5 + WL5*aL4;
% Output of Layer 5
HLS = ((ZL5 + 1)/2)*(HLSmax-HLSmin) + HLSmin;

```

### Abbreviations

$HLS$	Slug liquid holdup
$H_{LF}$	Film liquid holdup
$V_{SL}$	Superficial liquid velocity
$V_{SG}$	Superficial gas velocity
$V_M$	Mixture velocity
$E_1$	Average percent error, %
$\mu_L$	Liquid viscosity
$\mu_g$	Gas viscosity
$\theta$	Pipe inclination angle
$\theta_R$	Is the inclination angle from the horizontal in radians
$N_{Resl}$	Slug Reynold's number
$V_T$	Translational velocity
$E_2$	Absolute average percent error, %
$V_{BR}$	Bubble rise velocity
$d_b$	Bubble diameter
$d$	Pipe internal diameter
$\sigma_L$	Surface tension
$E_3$	Percent standard deviation, %
$\rho_L$	Liquid density
$\rho_G$	Gas density
$e_i$	Actual error
$\Delta\rho$	Change in density

$e_{ri}$	Relative error
R	Correlation coefficient
$E_{rms}$	Root-mean-square error
$F_{rp}$	Relative performance factor
$N_{Fr}$	Wallis (1969) dimensionless Froude number
$N_{\mu}$	Viscosity number
$N_f$	Inverse of the viscosity number
$N_{LV}$	Liquid velocity number
$E_4$	Average error
$N_{GV}$	Gas velocity number
$N_d$	Pipe diameter number
$N_L$	Liquid viscosity number
$E_5$	Absolute average error
$\bar{H}_{LSmeas}$	Average measured slug liquid holdup
$H_{LSmeas}$	Measured liquid holdup
$H_{LSpred}$	Predicted liquid holdup
$E_6$	Standard deviation
$\Delta \bar{e}_{imeas}$	Average change in measured liquid holdup
$X$	Input vector of five variables
$X_{(-1:1)}$	Input vector normalized in the range $\{-1, +1\}$
$X_{min}$	Minimum training dataset input vector as shown in column 4 of Table 3
$X_{max}$	Maximum training dataset input vector as shown in column 5 of Table 3
$Z^{L2}, Z^{L3}, Z^{L4}, Z^{L5}$	Net input vector into the second, third, fourth, and fifth layers, respectively
$b^{L2}, b^{L3}, b^{L4}, b^{L5}$	Bias vector of the second, third, fourth, and fifth layers, respectively
$a^{L1}, a^{L2}, a^{L3}, a^{L4}$	Activation vector of the second, third, and fourth layers, respectively
$w^{L2}, w^{L3}, w^{L4}, w^{L5}$	Weight matrix of the second, third, fourth, and fifth layers, respectively
ML	Machine learning
ANN	Artificial neural network
SLH	Slug liquid holdup
VMM	Visible mathematical model

#### Acknowledgements

Not applicable.

#### Authors' contributions

CCN, software, data curation, conceptualization, methodology, writing—original draft, formal analysis, investigation, and validation. UID, conceptualization, methodology, formal analysis, writing—review and editing, and supervision. CICA, writing—review and editing and supervision. AIBE, writing—review and editing and supervision. SIO, writing—review and editing. ANN, writing—review and editing. BUO, writing—review and editing. All authors have read and approved the manuscript.

#### Funding

The authors declare that no funding has been received from any organization/funding source as research assistance for current research.

#### Availability of data and materials

The datasets used and/or analyzed during the current study are available from the corresponding author on reasonable request.

#### Declarations

##### Competing interests

The authors declare that they have no competing interests.

Received: 9 February 2024 Accepted: 17 September 2024

Published online: 01 October 2024

#### References

1. Kanin EA, Osipov AA, Vainshtein AL, Burnaev EV (2019) A predictive model for steady-state multiphase pipe flow: machine learning on lab data. *J Pet Sci Eng* 180:727–746. <https://doi.org/10.1016/j.petrol.2019.05.055>
2. Kaya AS, Sarica C, Brill JP (1999) Comprehensive Mechanistic Modeling of Two-Phase Flow in Deviated Wells. SPE Annual Technical Conference and Exhibition, Houston, Texas, 3–6 October 1999. <https://doi.org/10.2118/56522-MS>
3. Kaya AS, Sarica C, Brill JP (2001) Mechanistic modeling of two-phase flow in deviated wells. *SPE Prod Facil* 16:156–165. <https://doi.org/10.2118/72998-PA>
4. Dukler AE, Hubbard MG (1975) A model for gas–liquid slug flow in horizontal and near horizontal tubes. *Ind Eng Chem Fundam* 14:337–347. <https://doi.org/10.1021/i160056a011>
5. Taitel Y, Bornea D, Dukler AE (1980) Modelling flow pattern transitions for steady upward gas–liquid flow in vertical tubes. *AIChE J* 26:345–354. <https://doi.org/10.1002/aic.690260304>

6. Barnea D, Shoham O, Taitel Y, Dukler AE (1985) Gas-liquid flow in inclined tubes: flow pattern transitions for upward flow. *Chem Eng Sci* 40:131–136. [https://doi.org/10.1016/0009-2509\(85\)85053-3](https://doi.org/10.1016/0009-2509(85)85053-3)
7. Petalas N, Aziz K (2000) Mechanistic model for multiphase flow in pipes. *J Can Pet Technol* 39:43–55. <https://doi.org/10.2118/00-06-04>
8. Taitel Y, Dukler AE (1976) A model for predicting flow regime transitions in horizontal and near horizontal gas-liquid flow. *AIChE J* 22:47–55. <https://doi.org/10.1002/aic.690220105>
9. Barnea D, Shoham O, Taitel Y (1982) Flow pattern transition for vertical downward two phase flow. *Chem Eng Sci* 37:741–744. [https://doi.org/10.1016/0009-2509\(82\)85034-3](https://doi.org/10.1016/0009-2509(82)85034-3)
10. Barnea D, Shoham O, Taitel Y (1982) Flow pattern transition for downward inclined two phase flow; Horizontal to vertical. *Chem Eng Sci* 37:735–740. [https://doi.org/10.1016/0009-2509\(82\)85033-1](https://doi.org/10.1016/0009-2509(82)85033-1)
11. Abdul-Majeed GH, Al-Mashat AM (2000) A mechanistic model for vertical and inclined two-phase slug flow. *J Pet Sci Eng* 27:59–67. [https://doi.org/10.1016/S0920-4105\(00\)00047-4](https://doi.org/10.1016/S0920-4105(00)00047-4)
12. Brill JP, Mukherjee H (1999) Multiphase flow in wells. Society of Petroleum Engineers, Richardson, TX, Richardson, Texas
13. Ali SF (2009) Two Phase Flow in Large Diameter Vertical Riser. In PhD Thesis. Cranfield University, Bedford, United Kingdom.
14. Kaya AS (1998) Comprehensive mechanistic modeling of two-phase flow in deviated wells. In PhD Thesis. The University of Tulsa, Tulsa, OK. <https://doi.org/10.1037//0033-2909.126.1.78>
15. Nwanwe CC, Duru UI, Nwanwe OI et al (2020) Optimum tubing size prediction model for vertical multiphase flow during flow production period of oil wells. *J Pet Explor Prod Technol* 10:2989–3005. <https://doi.org/10.1007/s13202-020-00964-8>
16. Ansari AM, Sylvester ND, Akron U et al (1994) A comprehensive mechanistic model for upward two-phase flow in wellbores. *SPE Prod Facil* 9:143–152. <https://doi.org/10.2118/20630-PA>
17. Nwanwe CC, Duru UI (2022) Comparison and performance analysis of models for predicting multiphase flow behaviours in wellbores. *Int J Pet Geosci Eng* 2022:1–20
18. Abdul-Majeed GH (2000) Liquid slug holdup in horizontal and slightly inclined two-phase slug flow. *J Pet Sci Eng* 27:27–32. [https://doi.org/10.1016/S0920-4105\(99\)00056-x](https://doi.org/10.1016/S0920-4105(99)00056-x)
19. Abdul-Majeed GH, Al-Mashat AM (2019) A unified correlation for predicting slug liquid holdup in viscous two-phase flow for pipe inclination from horizontal to vertical. *SN Appl Sci* 1: <https://doi.org/10.1007/s42452-018-0081-0>
20. Al-Safran E, Kora C, Sarica C (2015) Prediction of slug liquid holdup in high viscosity liquid and gas two-phase flow in horizontal pipes. *J Pet Sci Eng* 133:566–575. <https://doi.org/10.1016/j.petrol.2015.06.032>
21. Archibong-Eso A, Okeke NE, Baba Y et al (2019) Estimating slug liquid holdup in high viscosity oil-gas two-phase flow. *Flow Meas Instrum* 65:22–32. <https://doi.org/10.1016/j.flowmeasinst.2018.10.027>
22. Gomez LE, Shoham O, Schmidt Z et al (2000) Unified mechanistic model for steady-state two-phase flow: horizontal to vertical upward flow. *SPE J* 5:339–350. <https://doi.org/10.2118/65705-PA>
23. Gregory GA, Nicholson MK, Aziz K (1978) Correlation of the liquid volume fraction in the slug for horizontal gas-liquid slug flow. *Int J Multiph Flow* 4:33–39. [https://doi.org/10.1016/0301-9322\(78\)90023-X](https://doi.org/10.1016/0301-9322(78)90023-X)
24. Kora C, Sarica C, Zhang, HQ, Al-sarkhi, A, Alsafran, EM (2011) Effects of high oil viscosity on slug liquid holdup in horizontal pipes. Society of Petroleum Engineers - Canadian Unconventional Resources Conference 2011, CURC 2011:338–352.
25. Al-Safran E (2009) Prediction of slug liquid holdup in horizontal pipes. *J Energy Resour Technol Trans ASME* 131:0230011–0230018. <https://doi.org/10.1115/1.3120305>
26. Fernandes RC, Semiat R, Dukler AE (1983) Hydrodynamic model for gas-liquid slug flow in vertical tubes. *AIChE J* 29:981–989. <https://doi.org/10.1002/aic.690290617>
27. Zhang HQ, Qian W, Sarica C, Brill JP (2003) A unified mechanistic model for slug liquid holdup and transition between slug and dispersed bubble flows. *Int J Multiph Flow* 29:97–107. [https://doi.org/10.1016/S0301-9322\(02\)00111-8](https://doi.org/10.1016/S0301-9322(02)00111-8)
28. Barnea D, Brauner N (1985) Holdup of the liquid slug in two phase intermittent flow. *Int J Multiph Flow* 11:43–49. [https://doi.org/10.1016/0301-9322\(85\)90004-7](https://doi.org/10.1016/0301-9322(85)90004-7)
29. Kim TW, Kim S, Lim JT (2020) Modeling and prediction of slug characteristics utilizing data-driven machine-learning methodology. *J Pet Sci Eng* 195:107712. <https://doi.org/10.1016/j.petrol.2020.107712>
30. Abdul-Majeed GH, Kadhim FS, Almahdawi FHM et al (2022) Application of artificial neural network to predict slug liquid holdup. *Int J Multiph Flow* 150:104004. <https://doi.org/10.1016/j.ijmultiphaseflow.2022.104004>
31. Sylvester ND (1987) A mechanistic model for two-phase vertical slug flow in pipes. *J Energy Resour Technol Trans ASME* 109:206–213. <https://doi.org/10.1115/1.3231348>
32. Felizola H (1992) Slug Flow in Extended Reach Directional Wells. In MSc Thesis. The University of Tulsa, Tulsa, OK.
33. Gomez LE, Shoham O, Taitel Y (2000) Prediction of slug liquid holdup: horizontal to upward vertical flow. *Int J Multiph Flow* 26:517–521. [https://doi.org/10.1016/S0301-9322\(99\)00025-7](https://doi.org/10.1016/S0301-9322(99)00025-7)
34. Al-Ruhaimani F, Pereyra E, Sarica C et al (2018) Prediction of slug-liquid holdup for high-viscosity oils in upward gas/liquid vertical-pipe flow. *SPE Prod Oper* 33:281–299. <https://doi.org/10.2118/187957-pa>
35. Nwanwe CC, Duru UI, Anyadiegwu C, Ekejuba AIB (2023) An artificial neural network visible mathematical model for real-time prediction of multiphase flowing bottom-hole pressure in wellbores. *Pet Res* 8:370–385. <https://doi.org/10.1016/j.ptlrs.2022.10.004>
36. Tariq Z, Mahmoud M, Abdurraheem A (2020) Real-time prognosis of flowing bottom-hole pressure in a vertical well for a multiphase flow using computational intelligence techniques. *J Pet Explor Prod Technol* 10:1411–1428. <https://doi.org/10.1007/s13202-019-0728-4>
37. Gomaa I, Gowida A, Elkhatry S, Abdurraheem A (2021) The prediction of wellhead pressure for multiphase flow of vertical wells using artificial neural networks. *Arab J Geosci* 14:1–10. <https://doi.org/10.1007/s12517-021-07099-y>
38. Nwanwe CC, Duru UI (2023) An adaptive neuro-fuzzy inference system white-box model for real-time multiphase flowing bottom-hole pressure prediction in wellbores. *Petroleum* 9:629–646. <https://doi.org/10.1016/j.petlm.2023.03.003>
39. Abdul-Majeed GH (2022) Slug liquid holdup. *Mendeley Data V1*: <https://doi.org/10.17632/wyfdm5ysh6.1>
40. Ros NCJ (1961) Simultaneous flow of gas and liquid as encountered in well tubing. *J Pet Technol* 13:1037–1049. <https://doi.org/10.2118/18-PA>

41. Wallis GB (1969) One-dimensional two-phase flow. McGraw-Hill Book Co., Inc, New York City, New York City
42. Al-Naser M, Elshafei M, Al-Sarkhi A (2016) Artificial neural network application for multiphase flow patterns detection: a new approach. *J Pet Sci Eng* 145:548–564. <https://doi.org/10.1016/j.petrol.2016.06.029>
43. AlSaif A, Al-Sarkhi A, Ismaila K, Abdulkadir M (2022) Road map to develop an artificial neural network to predict two-phase flow regime in inclined pipes. *J Pet Sci Eng* 217:110877. <https://doi.org/10.1016/j.petrol.2022.110877>
44. Beale MH, Hagan MT, Demuth HB (2010) *Neural Network Toolbox™ 7 User's Guide*. The MathWorks, Inc., Natick, MA.
45. Baba YD, Aliyu AM, Archibong AE et al (2017) Study of high viscous multiphase phase flow in a horizontal pipe. *Heat Mass Transf* 54:651–669. <https://doi.org/10.1007/s00231-017-2158-5>
46. Wu B, Firouzi M, Mitchell T et al (2017) A critical review of flow maps for gas-liquid flows in vertical pipes and annuli. *Chem Eng J* 326:350–377. <https://doi.org/10.1016/j.cej.2017.05.135>
47. Kuncová G, Zahradník J (1995) Gas holdup and bubble frequency in a bubble column reactor containing viscous saccharose solutions. *Chem Eng Process Process Intensif* 34:25–34. [https://doi.org/10.1016/0255-2701\(94\)00563-X](https://doi.org/10.1016/0255-2701(94)00563-X)
48. Eissa SH, Schügerl K (1975) Holdup and backmixing investigations in cocurrent and countercurrent bubble columns. *Chem Eng Sci* 30:1251–1256. [https://doi.org/10.1016/0009-2509\(75\)85048-2](https://doi.org/10.1016/0009-2509(75)85048-2)
49. Wen Y, Wu Z, Wang J, et al (2017) Experimental study of liquid holdup of liquid-gas two-phase flow in horizontal and inclined pipes. *Int J Heat Technol* 35:713–720. <https://doi.org/10.18280/ijht.350404>
50. Andreussi P, Bendiksen K (1989) An investigation of void fraction in liquid slugs for horizontal and inclined gas-liquid pipe flow. *Int J Multiph Flow* 15:937–946. [https://doi.org/10.1016/0301-9322\(89\)90022-0](https://doi.org/10.1016/0301-9322(89)90022-0)
51. Godbole SP, Honath MF, Shah YT (1982) Holdup structure in highly viscous newtonian and non-Newtonian liquids in bubble columns. *Chem Eng Commun* 16:119–134. <https://doi.org/10.1080/00986448208911090>
52. Brauner N, Ullmann A (2004) Modelling of gas entrainment from Taylor bubbles. Part A: slug flow. *Int J Multiph Flow* 30:239–272. <https://doi.org/10.1016/j.ijmultiphaseflow.2003.11.007>

### **Publisher's Note**

Springer Nature remains neutral with regard to jurisdictional claims in published maps and institutional affiliations.